

How runoff begins (and ends): Characterizing hydrologic response at the catchment scale

Benjamin B. Mirus^{1,2} and Keith Loague¹

Received 17 March 2012; revised 19 March 2013; accepted 24 March 2013.

[1] Improved understanding of the complex dynamics associated with spatially and temporally variable runoff response is needed to better understand the hydrology component of interdisciplinary problems. The objective of this study was to quantitatively characterize the environmental controls on runoff generation for the range of different streamflow-generation mechanisms illustrated in the classic Dunne diagram. The comprehensive physics-based model of coupled surface-subsurface flow, InHM, is employed in a heuristic mode. InHM has been employed previously to successfully simulate the observed hydrologic response at four diverse, well-characterized catchments, which provides the foundation for this study. The C3 and CB catchments are located within steep, forested terrain; the TW and R5 catchments are located in gently sloping rangeland. The InHM boundary-value problems for these four catchments provide the corner-stones for alternative simulation scenarios designed to address the question of how runoff begins (and ends). Simulated rainfall-runoff events are used to systematically explore the impact of soil-hydraulic properties and rainfall characteristics. This approach facilitates quantitative analysis of both integrated and distributed hydrologic responses at high-spatial and temporal resolution over the wide range of environmental conditions represented by the four catchments. The results from 140 unique simulation scenarios illustrate how rainfall intensity/depth, subsurface permeability contrasts, characteristic curve shapes, and topography provide important controls on the hydrologic-response dynamics. The processes by which runoff begins (and ends) are shown, in large part, to be defined by the relative rates of rainfall, infiltration, lateral flow convergence, and storage dynamics within the variably saturated soil layers.

Citation: Mirus, B. B., and K. Loague (2013), How runoff begins (and ends): Characterizing hydrologic response at the catchment scale, *Water Resour. Res.*, 49, doi:10.1002/wrcr.20218.

1. Introduction

[2] The interactions between geology, climate, pedogenic maturity, geomorphology, vegetation, and land-use all pivot around the flow of water over the surface and within the near surface. Quantitative characterization of runoff processes is important for assessing threats to critical habitat, designing civil infrastructure, reducing the spread of non-point source contaminants, evaluating best management practices, soil conservation, and many other environmental problems. The arduous nature of characterizing runoff generation in the field has led to the widespread use of the dominant process concept and single-process models for interdisciplinary studies. The common simplifying assump-

tions of these models, such as reduced dimensionality, steady-state approximations, and indirect coupling of surface and subsurface water interactions, lead to misrepresentation of important processes such as flow convergence, transient response dynamics, and run-on. Furthermore, these assumptions allow only limited insight into internal catchment dynamics and spatial patterns that are crucial for evaluating water, solute, and sediment fluxes.

[3] Although gravity drives flow down topographic and hydrologic gradients, it remains difficult to characterize dynamic runoff-generation processes using only topographic characteristics such as slope, drainage area, and unit contour lengths. Regardless, the topographic index concept [Beven and Kirkby, 1979] is widely applied to represent hydrologic response; replacing the partial-differential equations describing fluid flow through variably saturated porous media with relatively simple topographic indices. Although there are limits to which topographic index models should be applied [Beven, 1997], simplifications are ultimately necessary for scaling-up hydrologic response to larger spatial and temporal scales needed to simulate processes such as landscape evolution [Dietrich *et al.*, 2003]. For example, Tucker and Bras [1998] used a landscape evolution model with simplified hydrology to

¹Department of Geological and Environmental Sciences, Stanford University, Stanford, California, USA.

²Now at U.S. Geological Survey, Menlo Park, California, USA.

Corresponding author: B. B. Mirus, Department of Geological and Environmental Sciences, Stanford University, Stanford, CA 94025, USA. (bbmirus@usgs.gov)

demonstrate the influence of different dominant runoff-generation mechanisms on drainage density and landscape morphology. Intuitively, environments dominated by Horton (infiltration excess) overland flow [Horton, 1945] and Dunne (saturation excess) overland flow [Dunne and Black, 1970a, 1970b] should support contrasting landscape morphologies and different critical habitats. However, progress in hydrogeomorphology and hydroecology has been hampered by a lack of quantitative understanding of linkages between the physical processes over the scales at which they occur [Sidle and Onda, 2004; Loague et al., 2006]. Dating back to Grove Karl Gilbert and Robert Elmer Horton, an important question has been where and by what processes do stream channels begin. The effort here focuses on the related question of how runoff begins (and ends). This study builds upon decades of foundational research on streamflow generation [see review by Beven, 2006] and rainfall-runoff modeling [see review by Loague, 2010].

[4] Figure 1 summarizes the occurrence of runoff-generation mechanisms in relation to their major environmental controls. Figure 1 is a modified version of the schematic illustration often referred to as the *Dunne diagram*. The original Dunne diagram was based upon accumulated insights from numerous field investigations of a variety of catchments throughout the world. Figure 1 qualitatively illustrates conditions for the occurrence of different runoff generation mechanisms, including subsurface stormflow (SSSF), Horton overland flow (HOF), and Dunne overland flow (DOF). Quantitative characterization of the physical controls on runoff generation is, however, lacking in Figure 1. The question of how runoff begins (and ends), therefore begs consideration using a quantitative, physically based approach.

[5] The motivation for this work was to begin developing a quantitative version of the Dunne diagram, which would enable graphical cataloguing of catchments based on measurable characteristics, such as topography, permeability, and soil depth. The objective of this study was to examine the

controls on runoff generation for a range of realistic environmental conditions using rigorous numerical simulations based on well-characterized experimental catchments.

2. The Integrated Hydrology Model (InHM)

[6] At the heart of this effort is the physics-based Integrated Hydrology Model (InHM), which was developed [VanderKwaak, 1999] to simulate fully coupled 3-D variably saturated flow in the subsurface and 2-D flow over the surface and in channels. InHM was selected for this study because there are no a priori specifications of a dominant runoff-generation mechanism, which facilitates a framework for addressing questions related to how soil-hydraulic properties and rainfall characteristics influence the location and timing of runoff generation. The equations and a detailed description of InHM are provided elsewhere [VanderKwaak, 1999; VanderKwaak and Loague, 2001].

3. Concept-Development Simulations

[7] The concept-development approach to improve process understanding was pioneered by Stephenson and Freeze [1974]. The InHM simulations in this study were developed on a foundation of distributed surface and near-surface hydrologic-response measurements for the experimental catchments known as C3 [Dutton et al., 2005; Mirus et al., 2007], CB [Ebel et al., 2007a, 2007b], TW [Western and Grayson, 1998; Mirus et al., 2009a], and R5 [Heppner et al., 2007, Heppner and Loague, 2008]. The C3 and CB catchments are located within steep, forested terrain where runoff generation is dominated by SSSF; the TW and R5 catchments are located in gently sloping rangeland where runoff generation is predominantly overland flow. Previously, Mirus et al. [2011a] investigated the bias introduced by contrasting degrees of observational detail from these four different experimental catchments based on InHM simulated hydrologic responses. Event-based simulations illustrate that the dominant processes were relatively unaffected by observed spatial variability in soil depth, saturated hydraulic conductivity, and rainfall intensity within individual catchments. Ultimately, Mirus et al. [2011a] established a common level of boundary-value problem (BVP) complexity for the four catchments. Each of the four BVPs consists of several uniform, homogenous, isotropic hydrogeologic units and employs a spatially uniform rainfall boundary condition. Further details on grid spacing, boundary conditions, and the distributed data sets employed to derive model parameters for each BVP are provided in Mirus et al. [2011a]. The common level of BVP complexity facilitates an unbiased comparison of how equivalent changes in hydraulic properties and rainfall intensity affect hydrologic responses across all four catchments.

[8] The work presented here employs the four BVPs from Mirus et al. [2011a] as the *base-case* scenarios for concept-development simulations, designed to investigate runoff generation mechanisms within a physically realistic range of soil-hydraulic properties and rainfall characteristics. With the four base-case BVPs as a starting point, systematic changes in parameter values and applied flux boundary conditions are used to establish *alternative* scenarios to examine the controls on runoff generation. The

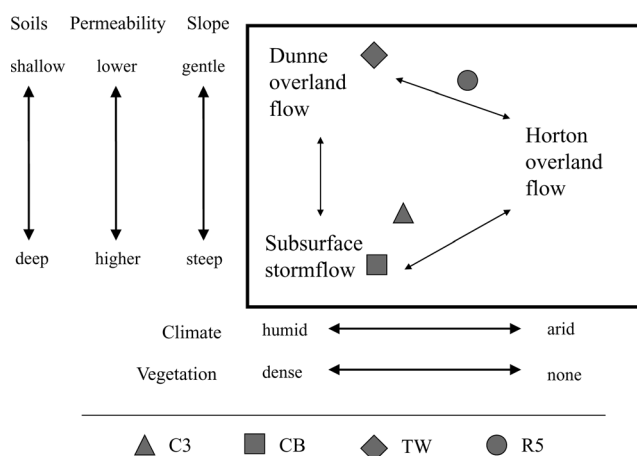


Figure 1. A modified version of the Dunne diagram, illustrating environmental controls on the different runoff-generation mechanisms [after Dunne, 1978]. The C3, CB, TW, and R5 catchments are plotted according to the dominant runoff response observed at each location [from Mirus et al., 2011a].

alternative scenarios are treated as hypothetical realities [e.g., *Mirus et al.*, 2011b] designed to explore a range of environmental conditions.

3.1. Base Cases

[9] The characteristics of the base-case BVPs for C3, CB, TW, and R5, which include boundary conditions, initial conditions, topography, surface properties, and soil-hydraulic properties, are taken directly from *Mirus et al.* [2011a]. These four catchments are plotted in terms of dominant runoff generation mechanisms in Figure 1. The average slopes represented by the four topographies spans the range of what can be expected to occur in soil-mantled landscapes from the low gradients at TW and R5 (2° and 3° , respectively) to moderate and very steep slopes at C3 and CB (18° and 43° , respectively). The topography for each catchment (shown in Figure 2) remains constant throughout the alternative simulation scenarios developed here to isolate the influence of hydraulic properties and rainfall on runoff generation for individual storm events.

3.2. Defining the Parameter Space

[10] The parameter space explored for the concept-development simulations reported here is defined by the overall range of parameter values and rainfall characteristics for the four base-case BVPs. Table 1 provides both the hydraulic property values for the different units in each base case, and the range in values across all four cases used in the concept-development simulations. The soil-water retention and hydraulic conductivity characteristic curves, for the soils summarized in Table 1, are shown in Figure 3. Each alternative simulation scenario consists of a bedrock unit overlain by one, two, or three soil units, and the combination of parameter values for each soil unit results in characteristic curves that fall within the respective upper and lower bounds shown in Figure 3. The range of rainfall characteristics for the alternative simulation scenarios were gleaned from the ensemble of the long-term rainfall records from the four experimental catchments [see *Ebel et al.*, 2007a; *Heppner et al.*, 2007; *Mirus et al.*, 2007, 2009a].

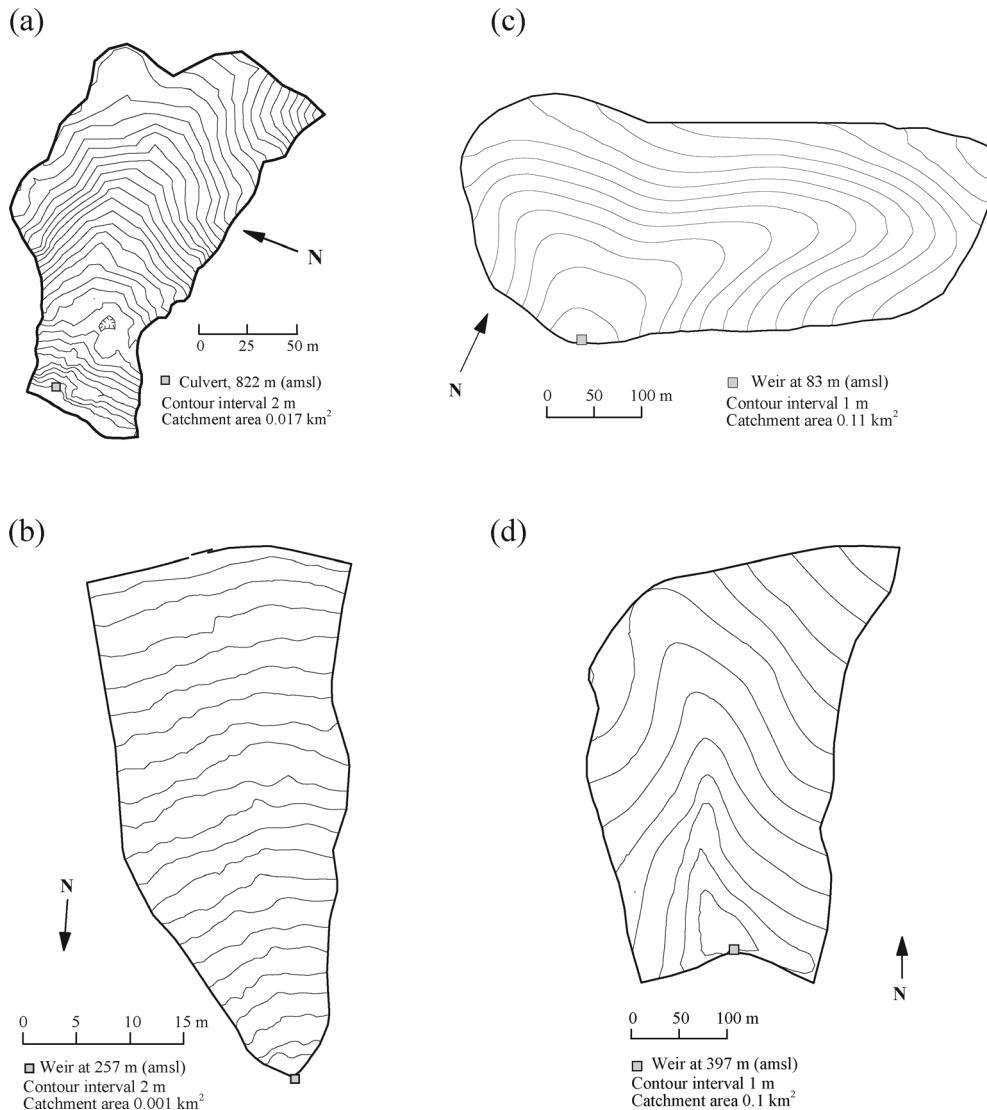
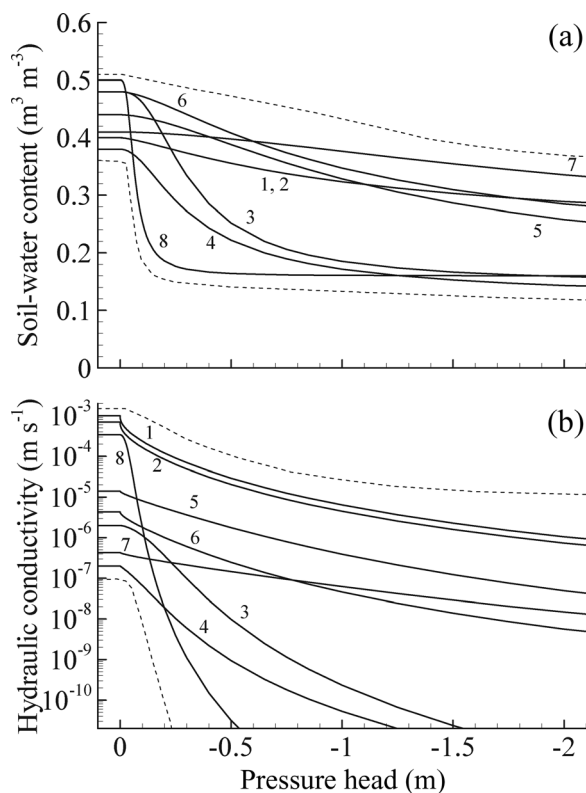


Figure 2. Topography of (a) C3, (b) CB, (c) TW, and (d) R5.

Table 1. Parameter Values for Base-Cases [from *Mirus et al.*, 2011a, 2011b, 2011c] and Concept-Development Simulations in This Study

Characteristic curves ^a	Catchment	Unit ^b	b (m) ^c	K_{sat} (m s ⁻¹) ^d	n (-) ^e	α (m ⁻¹) ^f	β (-) ^f	θ_{res} (-) ^g
1 ^a	C3	TS	1.50	1.0×10^{-3}	0.40	2.0	1.3	0.15
2 ^a	C3	S1	1.50	7.0×10^{-4}	0.40	2.0	1.3	0.15
3 ^a	TW	TS	0.23	2.0×10^{-6}	0.48	4.0	2.5	0.14
4 ^a	TW	S1	1.00	2.0×10^{-7}	0.38	4.5	2.0	0.11
5 ^a	R5	TS	0.20	1.4×10^{-5}	0.44	1.3	1.7	0.09
6 ^a	R5	S1	0.20	4.3×10^{-6}	0.48	1.8	1.6	0.13
7 ^a	R5	S2	1.40	4.3×10^{-7}	0.41	0.6	1.7	0.16
8 ^a	CB	TS	0.96	3.4×10^{-4}	0.50	35.0	3.0	0.16
9	C3	BR	100	1.0×10^{-9}	0.20	4.3	1.3	0.02
10	TW	BR	20	2.0×10^{-9}	0.20	6.0	1.5	0.02
11	R5	BR	5.0	4.6×10^{-9}	0.30	0.6	1.7	0.02
12	CB	S2	2.0	7.2×10^{-5}	0.15	4.3	1.3	0.01
13	CB	BR	53	5.0×10^{-7}	0.12	4.3	1.3	0.01
Parameter space								
Soil, maximum				1.0×10^{-3}	0.50	35.0	3.0	0.16
Soil, mean				1.3×10^{-5}	0.44	17.8	2.2	0.13
Soil, minimum				2.0×10^{-7}	0.38	0.6	1.3	0.09
Bedrock, maximum				5.0×10^{-7}	0.30	6.0	1.7	0.02
Bedrock, mean				2.2×10^{-8}	0.26	3.3	1.5	0.02
Bedrock, minimum				1.0×10^{-9}	0.12	0.6	1.3	0.01

^aSee Figure 3.^bHydrogeologic units: topsoil (TS), subsoil-1 (S1), subsoil-2 (S2), bedrock (BR).^cUnit thickness.^dSaturated hydraulic conductivity (isotropic).^ePorosity.^fCharacteristic curve shape parameters from *van Genuchten* [1980].^gResidual volumetric-water content.**Figure 3.** Characteristic curves for the different soil units in the base-case boundary value problems: (a) water retention, and (b) hydraulic conductivity. Parameter values are summarized in Table 1. The area within the dashed lines represents the range of the parameter space considered for the concept-development simulations.

The impact of evapotranspiration (ET) was not considered for the event-based simulations in this study.

3.3. Alternative Simulation Scenarios

[11] The alternative scenarios were generated in two phases; the simulations in Phases I and II are focused on impacts to runoff-generation related to changes in soil-hydraulic properties and rainfall characteristics of the base cases, respectively. Initial conditions for the event-based simulations were estimated by draining the catchment from near-saturation, followed by a “warm-up” rainfall simulation, using the protocol reported by *Mirus et al.* [2011a]. In Phases I and II there are 35 alternative simulation scenarios for each catchment in addition to the base case (i.e., scenario 0). These scenarios are numbered using the catchment name as a prefix; for example the base-case scenario for R5 is R5-0, whereas the third scenario for TW is TW-3.

[12] The Phase I scenarios were derived through an orderly series of changes in the individual soil-hydraulic property values with the same observed rainfall events presented in *Mirus et al.* [2011a]. The alternative scenarios examine the following four properties: saturated hydraulic conductivity (K_{sat}), the characteristic curve shape, defined using the *van Genuchten* [1980] parameters (α and β), porosity (n), and residual water content (θ_{res}). For each of these four properties, three alternative scenarios were derived to explore the upper, lower and middle range of parameter values for both the topsoil and subsoil-1 layers (see Table 1 and Figure 3). Table 2 lists the perturbed parameter values for the total of 24 alternative scenarios for each catchment in Phase I.

[13] The Phase II scenarios were derived by applying different rainfall events with the base-case parameterization of

Table 2. Soil-Hydraulic Property Values Assigned in Phase I

Scenario	Unit ^a	K_{sat} (m s ⁻¹) ^b	α (m ⁻¹) ^c	β (-) ^c	n (-) ^d	θ_{res} (-) ^e	Runoff ^f
0	NA	BC ^g	BC	BC	BC	BC	C3, R5
1	TS	1.0×10^{-3}	BC	BC	BC	BC	C3, R5
2	TS	2.5×10^{-5}	BC	BC	BC	BC	C3, R5
3	TS	2.0×10^{-7}	BC	BC	BC	BC	C3, R5
4	TS	BC	5.0	3.0	BC	BC	C3
5	TS	BC	1.7	2.0	BC	BC	C3, R5, CB
6	TS	BC	0.6	1.1	BC	BC	C3, R5, CB
7	TS	BC	BC	BC	0.50	BC	C3, R5
8	TS	BC	BC	BC	0.44	BC	C3, R5
9	TS	BC	BC	BC	0.38	BC	C3, R5
10	TS	BC	BC	BC	BC	0.17	C3, R5
11	TS	BC	BC	BC	BC	0.08	C3, R5
12	TS	BC	BC	BC	BC	0.04	C3, R5
13	S1	1.0×10^{-3}	BC	BC	BC	BC	R5
14	S1	2.5×10^{-5}	BC	BC	BC	BC	C3, R5
15	S1	2.0×10^{-7}	BC	BC	BC	BC	C3, R5
16	S1	BC	5.0	3.0	BC	BC	C3
17	S1	BC	1.7	2.0	BC	BC	C3, R5
18	S1	BC	0.6	1.1	BC	BC	C3, R5
19	S1	BC	BC	BC	0.50	BC	C3, R5
20	S1	BC	BC	BC	0.44	BC	C3, R5
21	S1	BC	BC	BC	0.38	BC	C3, R5
22	S1	BC	BC	BC	BC	0.17	C3, R5
23	S1	BC	BC	BC	BC	0.08	C3, R5
24	S1	BC	BC	BC	BC	0.04	C3, R5

^aHydrogeologic units: topsoil (TS), subsoil-1 (S1).

^bSaturated hydraulic conductivity.

^cCharacteristic curve shape parameter from *van Genuchten* [1980].

^dPorosity.

^eResidual volumetric-water content.

^fIndicates for which catchments runoff was produced.

^gBase case (BC) values for each catchment are given in Table 1.

hydrogeologic units for each catchment (Table 1). The alternative scenarios employ the four rainfall events from the base-case data sets [*Mirus et al.*, 2011a] applied to all four catchments, as well as several hypothetical, steady-intensity rainfall events. The hypothetical events were generated using individual event characteristics (i.e., peak intensity and total duration) that fall within the observed ranges from the long-term records of the four data sets [*Ebel et al.*, 2007a, *Heppner et al.*, 2007; *Mirus et al.*, 2007, 2009a]. For

example, scenario 27 applies the maximum peak intensity for the minimum duration from the event characteristics of the base-case BVPs. Table 3 summarizes the 11 real and hypothetical rainfall events that were considered in Phase II. The protocol for generating the alternative rainfall scenarios produces one duplicate of the base case for each catchment for the original observed rainfall event (i.e., C3–29, CB–30, TW–34, and R5–31), so a total of 10 unique simulations are considered for each catchment in Phase II.

Table 3. Characteristics of the Phase II Rainfall Events

Scenario	Total depth (mm)	Total duration (h)	Average intensity		Maximum intensity		Runoff ^a
			mm h ⁻¹	m s ⁻¹	mm h ⁻¹	m s ⁻¹	
25 ^b	2710	226	12.0	3.3×10^{-6}	12.0	3.3×10^{-6}	C3, R5, CB
26 ^b	452	226	2.0	5.6×10^{-7}	2.0	5.6×10^{-7}	C3, R5, CB
27 ^b	360	30	12.0	3.3×10^{-6}	12.0	3.3×10^{-6}	C3, R5, CB
28 ^b	304	4	76.3	2.1×10^{-5}	76.3	2.1×10^{-5}	C3, TW, R5, CB
29 ^c	286	226	1.3	3.5×10^{-7}	7.1	2.0×10^{-6}	C3, R5, CB
30 ^d	72	166	0.4	1.2×10^{-7}	2.0	5.6×10^{-7}	
31 ^e	50	3.6	13.9	3.9×10^{-6}	76.3	2.1×10^{-5}	R5
32 ^f	49	22	2.2	6.2×10^{-7}	13.2	3.7×10^{-6}	
33 ^b	48	2	12.0	3.3×10^{-6}	12.0	3.3×10^{-6}	R5
34 ^f	19	70	0.3	7.5×10^{-8}	2.8	7.8×10^{-7}	
35 ^f	14	39	0.4	1.0×10^{-7}	2.6	7.2×10^{-7}	

^aIndicates for which catchments runoff was produced.

^bSteady-intensity rainfall event generated from characteristics of the base-case rainfall events.

^cEvent from the observed C3 record [see *Mirus et al.*, 2007].

^dSprinkling experiment from the observed CB record [see *Ebel et al.*, 2007a].

^eEvent from the observed R5 record [see *Heppner et al.*, 2007].

^fEvent from the observed TW record [see *Mirus et al.*, 2009a].

4. Results

[14] Figure 4 presents the hydrologic-response for the C3 Phase I scenarios 0, 3, 13, and 15 (see Table 2). Figure 4 is introduced here as an example of the template employed consistently for displaying the simulation results in terms of both the integrated runoff response (discharge hydrograph) and distributed runoff response (spatial patterns of surface water flow). To facilitate clear discussion of certain

specific features of the distributed response, these snapshots are divided into four map-view quadrants when necessary (e.g., snapshot B₀).

4.1. Defining Surface Runoff

[15] One challenge with using hydrologic-response models like InHM in a concept-development mode is distinguishing between shallow overland flow and surface runoff. For

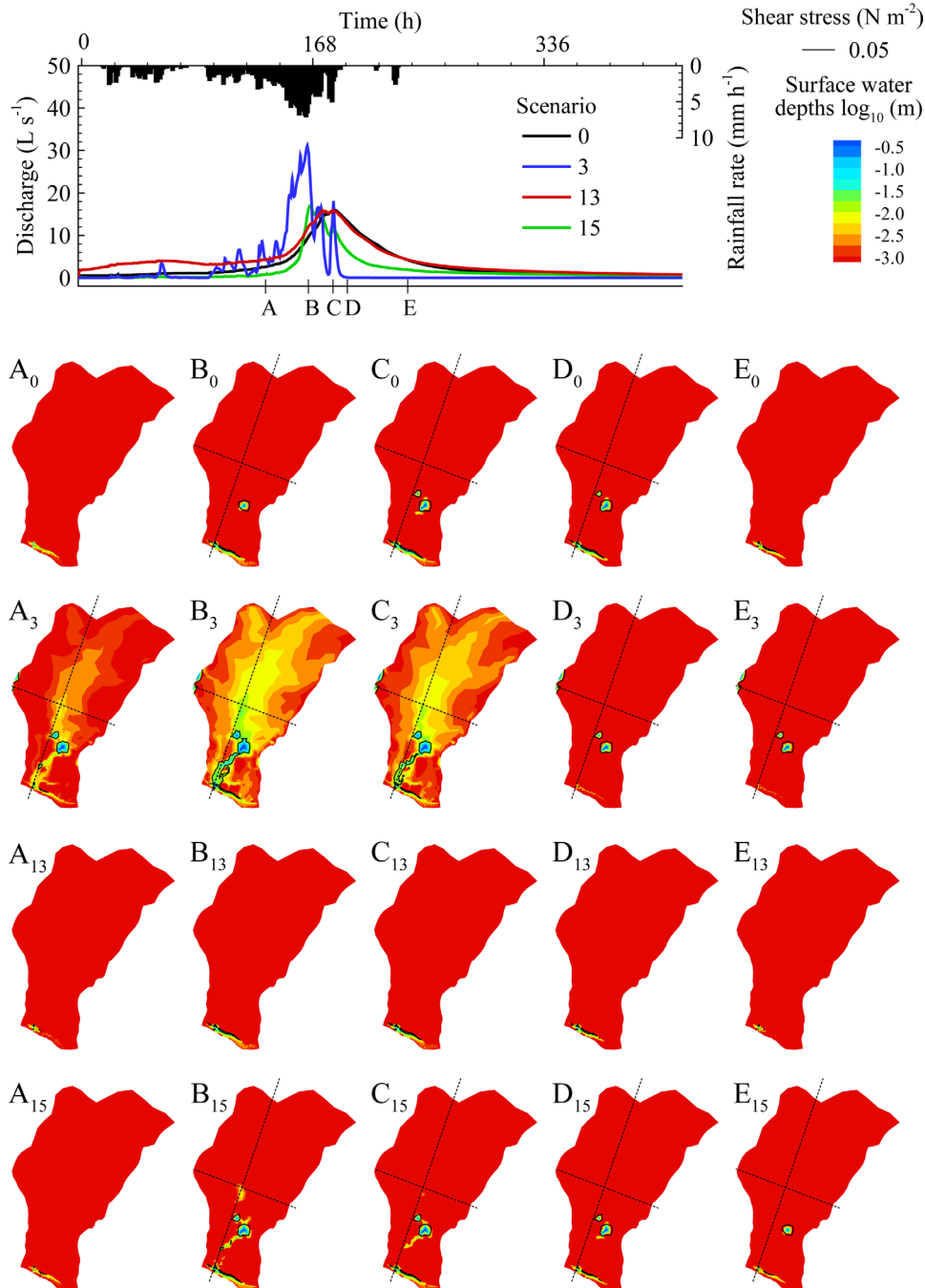


Figure 4. Simulated hydrologic response for C3 Phase I, scenarios 0, 3, 13, and 15 (Table 2). The upper portion shows the event hyetograph and hydrographs of the integrated responses with five output times indicated (A through E). The lower portion shows snapshots of the distributed responses at the five output times. Snapshot A₀ is simulated output time A for C3-0. Dashed lines dividing the catchment into four quadrants are provided as a visual aid to assist in descriptions.

example, InHM is capable of simulating runoff that would generally not be detected using standard field measurement techniques. Such very low-flow depths and velocities are of limited relevance in natural systems, with the exception of severely disturbed landscapes (e.g., postwildfire erosion). This challenge of identifying “relevant” runoff is further complicated when examining simulations for a range of different topographies and drainage areas, from the gently sloping R5 catchment to the extremely steep CB hillslope. Here shear stress at the base of overland flow is used to determine an appropriate threshold for identifying runoff because it provides an objective, physically based estimate of erosion potential and sediment transport capacity that accounts for topographic slope [e.g., Ritter *et al.*, 1978]. Critical shear stress represents the minimum transport capacity to begin entrainment for detached sediment of a specified density and grain size [Shields, 1936]. For this study, critical shear stress is calculated assuming a representative grain size of fine sand/silt using the simple protocol outlined by Soulsby [1997]. Details of the method for shear stress calculation, driven by the InHM simulated surface water depths and velocities are summarized by Mirus [2009].

[16] The simulated critical shear stress value is shown on the surface water depth snapshots using a single contour (see Figure 4), which is employed as an indicator of significant runoff. The region in which the critical shear stress is exceeded is henceforth referred to as *surface runoff*, distinguishing it from both deeper, relatively immobile water (i.e., ponds) and shallow overland flow traveling at much slower velocities (i.e., sheetwash). Although not the focus of this study, the impact of selecting alternative grain sizes as well as the other assumptions employed in the critical shear stress calculations and exceedance criteria are discussed by Mirus [2009]. This surface runoff metric facilitates an objective comparison of simulation results for the four different catchments.

[17] Three exceptions for the channelized runoff criteria described above are necessary to allow objective comparison of runoff generation across the different alternative scenarios. First, because of the steep slopes at CB (Figure 2b) any mobile surface water would be sufficient to exceed the critical shear stress for fine sand [Mirus, 2009], so the contour of the critical shear stress value is not shown on the figure of CB scenarios. Second, the C3 BVPs include an unpaved road along the downstream boundary of the catchment (Figure 2a). The effect of anthropogenic features is beyond the scope of this study, so any flow along the road and exfiltration from the steep road cut was not considered in determining the surface runoff criteria described above. Finally, the R5 BVPs employ topography that includes a constructed berm, which focuses runoff through the weir and results in a topographic depression just up-gradient of the catchment outlet (Figure 2d). The berm and pond affects the natural drainage, with the steep slopes on either side of the weir promoting rapid overland flow. As with the C3 road, the weir and berm at R5 introduce complications beyond the major focus of this study, so the region within the weir pond was not considered in determining the surface runoff criteria.

4.2. Simulated Runoff Generation

[18] The 49 Phase I and 18 Phase II scenarios that resulted in surface runoff, based upon the criteria in section

4.1 [also see Mirus, 2009], are listed in Tables 2 and 3, respectively. Examination of Tables 2 and 3 reveals the both expected and unexpected controls on runoff. The unsaturated zone hydraulic properties and subsoil-1 hydraulic conductivity, as well as the rainfall depth have a considerable influence for a range of different topographies. Although average rainfall intensities span two orders of magnitude fewer than the K_{sat} values considered in this study, perusal of Tables 2 and 3 suggests that rainfall intensity exerts a greater control on the occurrence of surface runoff than K_{sat} . Generally, when the average rainfall intensity exceeds the topsoil K_{sat} , surface runoff occurs for all four topographies. However, when the topsoil K_{sat} exceeds the average rainfall intensity there is no consistent trend in surface runoff occurrence (or lack thereof).

[19] Rainfall intensity does not have an impact on surface runoff for the CB and C3 scenarios, whose similarity in responses shown in Tables 2 and 3 suggests (confirms) that steep topography is an important control on runoff. Conversely, despite the similar slopes and drainage areas of TW and R5, the Phase I and II results (Tables 2 and 3) indicate disparate controls on runoff generation for the base-case BVPs and their derivative scenarios. The R5 scenarios each tend to produce surface runoff except under very low-intensity rainfall, whereas the TW scenarios produce surface runoff only for the very highest intensity rainfall events. A summary of the detailed analyses for the simulated hydrologic response from the Phase I and II scenarios is provided in the following subsections. Selected scenarios exhibiting notable differences from the base case are illustrated graphically and discussed. The primary controls on runoff response are summarized for each catchment.

4.2.1. C3 Scenarios

[20] Simulation results for selected C3 scenarios are shown in Figures 4 through 6, which reveal that many different combinations of integrated and distributed response are possible for the same topography. The majority of the scenarios in Phase I and II are dominated by SSSF due to the deep, permeable soils, low-rainfall intensities and the steep slopes. For most scenarios, the rainfall intensities are both several orders of magnitude below the saturated hydraulic conductivity of the soils, and at least one order of magnitude greater than the saturated hydraulic conductivity of the bedrock. For the scenarios dominated by SSSF (e.g., C3–13), the discharge hydrograph reflects the timing and quantity of exfiltration along the road. However, the discharge hydrograph is not a clear indicator of the distributed response or the active runoff generation mechanisms. While HOF occurs only when topsoil K_{sat} is set well below the rainfall intensity (Figure 4, C3-3), the break in slope along the catchment axis (see Figure 2a) provides conditions for the Dunne mechanism, which occurs in response to sustained rainfall for a variety of scenarios (Figure 4, scenarios C3-0 and C3–13; both scenarios in Figure 5). The maximum extent of DOF generally occurs during peak discharge, which is well after peak rainfall intensity (e.g., Figure 4, snapshot C₀; Figure 5 snapshot D₂₈). The onset of DOF is related to higher discharge at the outlet, and the hydrograph rises sharply when DOF contributes to the integrated response (e.g., Figure 5, compare snapshots A₂₇ and B₂₇). Discharge and DOF generally peak shortly after the rainfall ceases, then quickly recedes as the upper quadrants

MIRUS AND LOAGUE: HOW DOES RUNOFF BEGIN (AND END)?

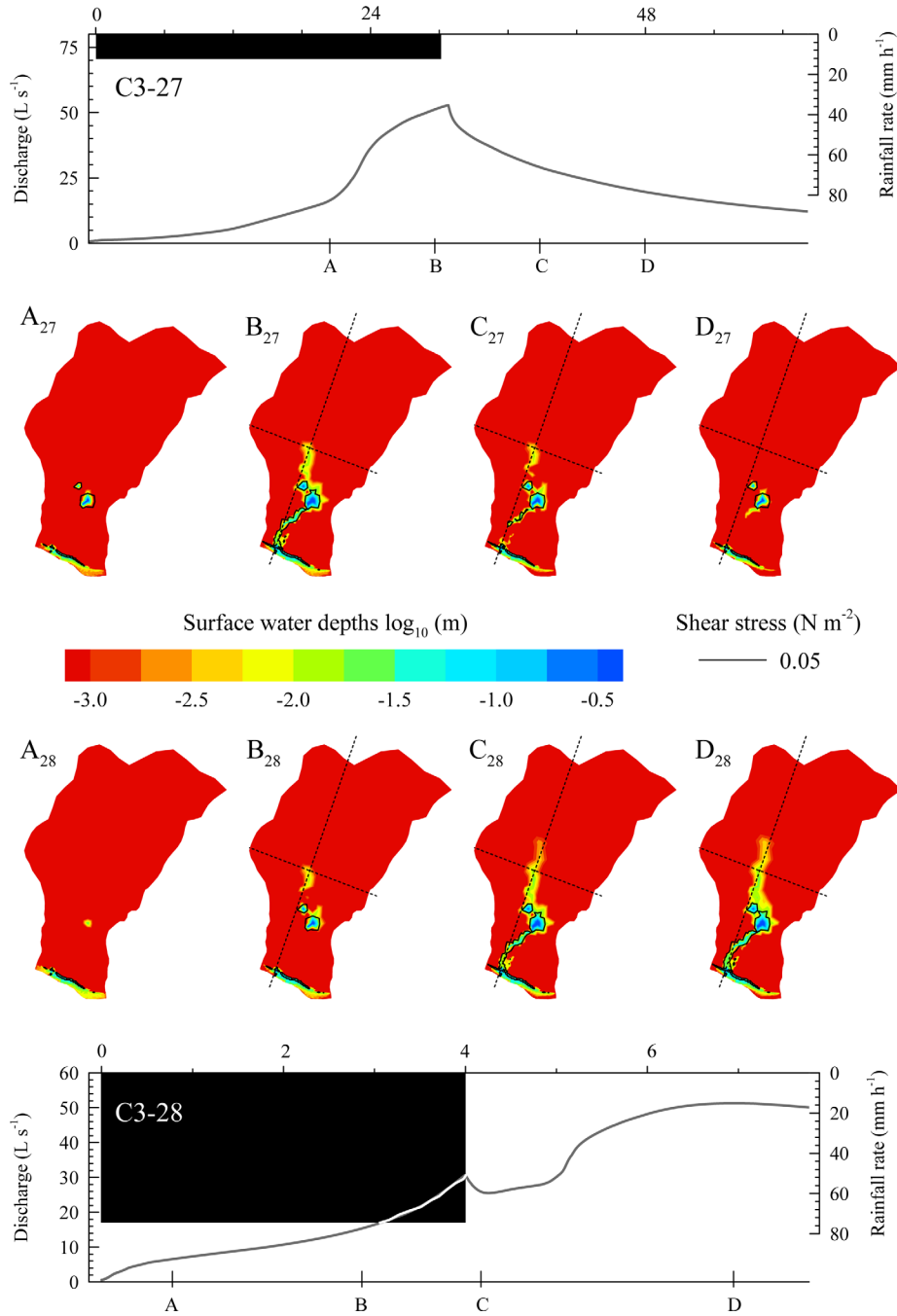


Figure 5. Simulated hydrologic response for C3 Phase II, scenarios 27 (upper) and 28 (lower) (Table 3). Dashed lines dividing the catchment into four quadrants are provided as a visual aid to assist in descriptions.

of the catchment drain (e.g., Figure 4, compare snapshots B_{15} and D_{15} ; Figure 5, compare snapshots B_{28} and D_{28}).

[21] Figure 6 shows the subsurface hydraulic-head distribution during peak discharge for the base case (Figure 4, snapshot C_0). Examination of Figure 6 reveals the complex, three-dimensional nature of the hydrologic response. Hydraulic-head gradients in the bedrock, underlying the break in the topography drive flow up toward the surface, which is consistent with established groundwater flow theory for topographic influence on discharge zones [Toth, 1963]. Total hydraulic-head gradients within the unsaturated

topsoil and across the soil-bedrock interface are vertical. In contrast, the head gradients in the variably saturated topsoil and subsoil-1, and deeper within the saturated bedrock are predominantly in the down-slope direction. Therefore, slope-parallel flow occurs both longitudinally, toward the down-gradient boundary (Figure 6b) and laterally, due to the convergent topography (Figure 6c). The asymmetry of the hydraulic-head distributions along the lateral transect (Figure 6c) illustrates the role of catchment shape and the assumptions of impermeable boundaries on constraining the subsurface flow system.

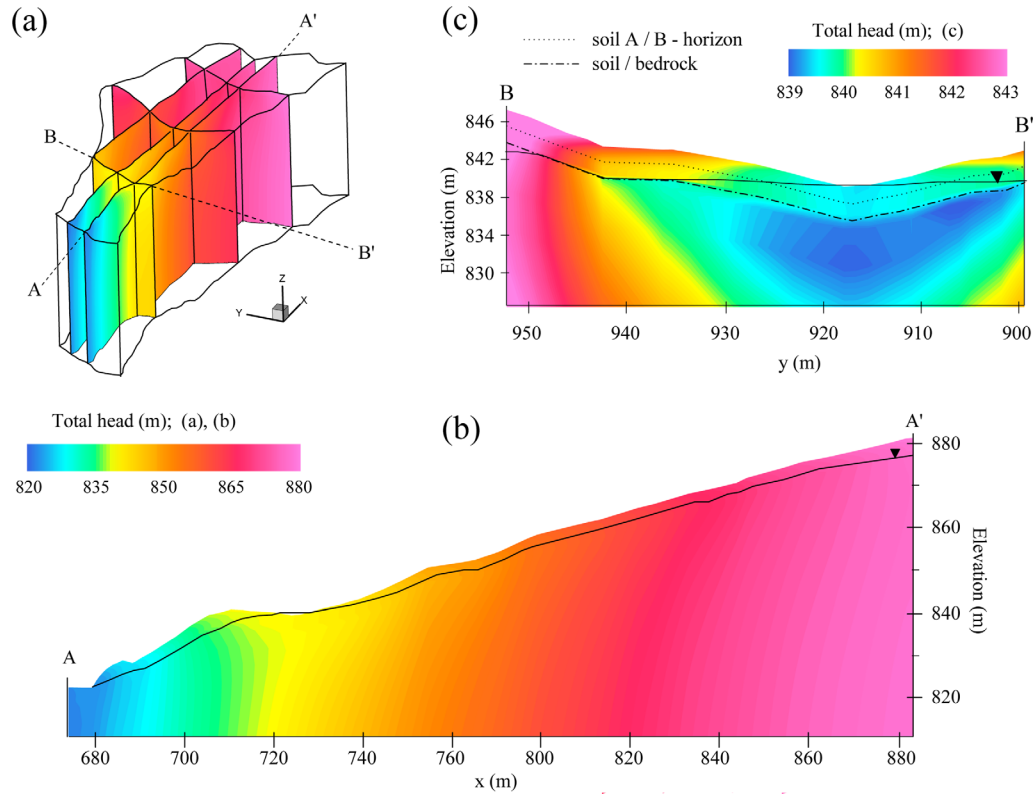


Figure 6. Subsurface hydraulic head distribution for the C3 base case at output time B (see Figure 4, snapshot B₀). (a) 3-D fence diagram of the entire catchment. (b) 2-D slice for the A-A' transect. (c) 2-D slice for the B-B' transect.

4.2.2. CB Scenarios

[22] The CB base case is dominated by SSSF with no runoff. Examination of Tables 2 and 3 reveals that many scenarios in Phases I and II respond identically to the base case. Simulation results for selected scenarios that exhibit an overland flow response are shown in Figure 7. Runoff generation for all the scenarios is dominated by the steep topography; SSSF velocities vary substantially between the scenarios depending upon the permeability contrasts between the hydrogeologic units [Mirus, 2009]. As with C3, the water table dynamics for the CB scenarios is controlled by the hydraulic conductivity and porosity of the soil units and the rainfall intensity. Scenarios that do result in overland flow are those with large total rainfall depths (i.e., scenarios CB-25 through CB-29) or decreased unsaturated zone storage (i.e., scenarios CB-5 and CB-6). For rainfall events where both the average intensity and total depth of rainfall are high enough to exceed the unsaturated storage, surface runoff dominates the integrated response. Additionally, the highly permeable soils and low-rainfall intensities of the base case preclude the occurrence of HOF within the framework employed in this study. DOF is generated when SSSF convergence promotes a rise of the water table to intersect the surface more rapidly than the permeable soils can drain laterally through the catchment outlet. This threshold for surface runoff is generally exceeded when average rainfall intensities are high for a period of time long enough (i.e., sufficient cumulative rainfall depth). Runoff begins and ends at the downstream boundary where a seepage face first develops due to the largest upslope contributing area. However, as

with the C3 scenarios, the topographic depressions (e.g., in the upper right-hand quadrant of snapshots) is also a starting and ending point for the occurrence of DOF (e.g., Figure 7, snapshots A₂₇ and A₂₈).

4.2.3. TW Scenarios

[23] Simulation results for selected TW scenarios are shown in Figures 8 and 9. The majority of the scenarios in Phase I and II are dominated by DOF due to the gentle slopes and shallow water table. Exfiltration of subsurface flow within the convergent topography occurs for all scenarios, but only dominates the response for very high-topsoil permeability (i.e., TW-1). Although HOF does occur when the topsoil saturated hydraulic conductivity is lower than the rainfall intensities (i.e., scenarios 3, 25, 27, 28, 31, and 33), the timing and spatial pattern of runoff are strongly influenced by the wet initial conditions [see Mirus *et al.*, 2011a]. Although overland flow occurs, the surface runoff threshold described in section 4.1 is not exceeded for the TW base case and many other scenarios (Tables 2 and 3).

[24] The runoff patterns for all TW scenarios reflect the two convergent hollows, which bifurcate in opposing directions from the catchment outlet (see Figure 2c). For a given scenario, comparison between the patterns of overland flow depths within the hollows reflects the different drainage areas contributing to DOF and subsurface exfiltration within each. As shown in Table 3, only the rainfall event with the highest average intensity resulted in surface runoff (TW-28), despite other events with greater total depth or equivalent peak intensity. The smooth and gently sloping topography (Figure 2c) favors the widening of overland

MIRUS AND LOAGUE: HOW DOES RUNOFF BEGIN (AND END)?

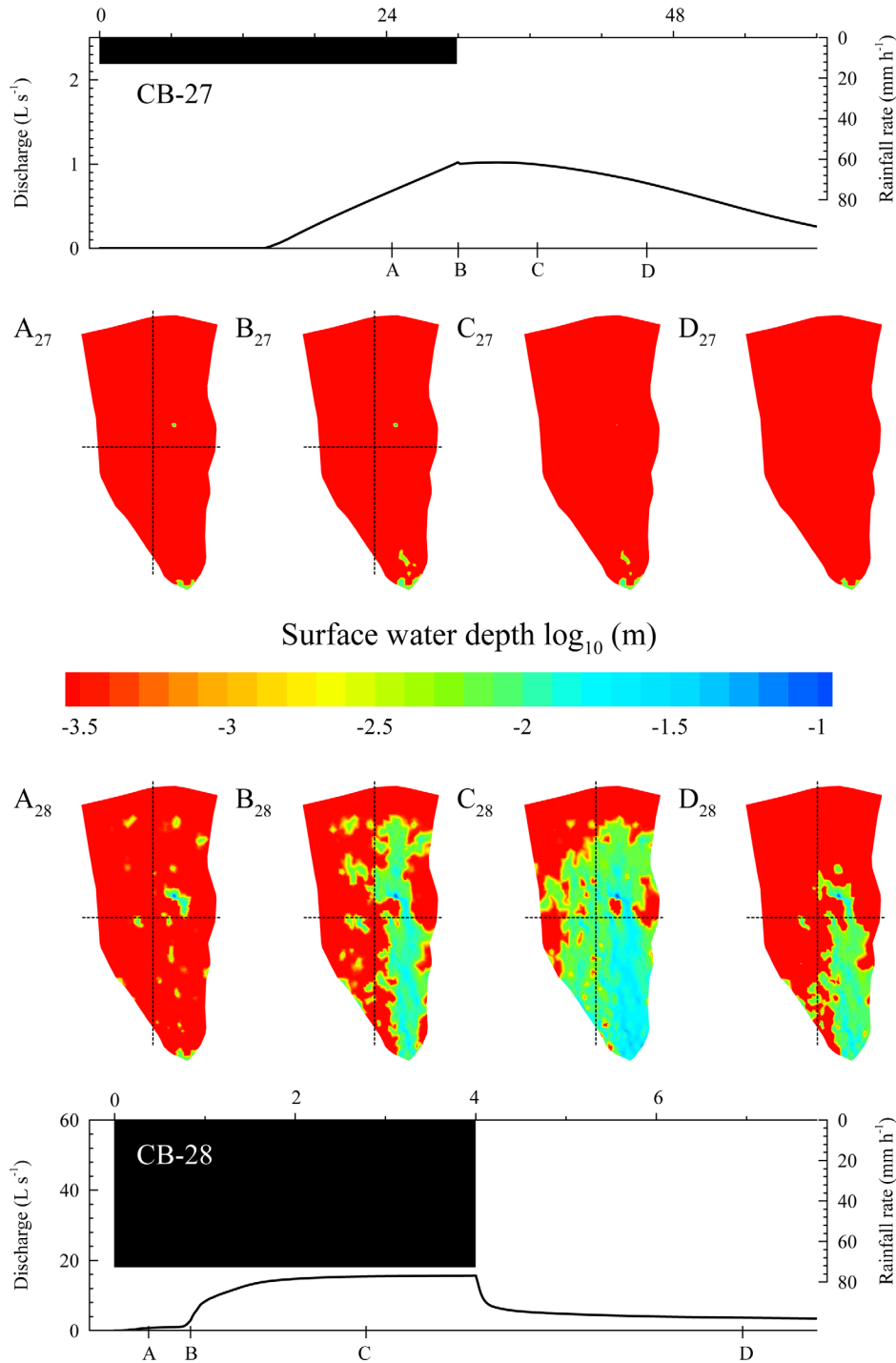


Figure 7. Simulated hydrologic response for CB Phase II, scenarios 27 (upper) and 28 (lower) (Table 3). Dashed lines dividing the catchment into four quadrants are provided as a visual aid to assist in descriptions.

flow to accommodate increased discharge (from overland flow convergence and exfiltration), instead of producing the deeper and/or more rapid response needed to meet the runoff criteria.

4.2.4. R5 Scenarios

[25] Simulation results for selected R5 scenarios are shown in Figure 10. Hydrologic response for most scenarios is dominated by a combination of HOF and DOF, where

the relative combination of each depends heavily on total rainfall depth, initial unsaturated storage, and subsurface permeability contrasts. The alternative scenarios from Phase I illustrated in Figure 10 provide examples of how the unsaturated zone storage and the relative rates of flow through the different hydrogeologic units affect discharge. However, for scenarios 1, 13, and 15 the overall runoff patterns are quite similar to the base case. Scenarios with high-rainfall intensity

MIRUS AND LOAGUE: HOW DOES RUNOFF BEGIN (AND END)?

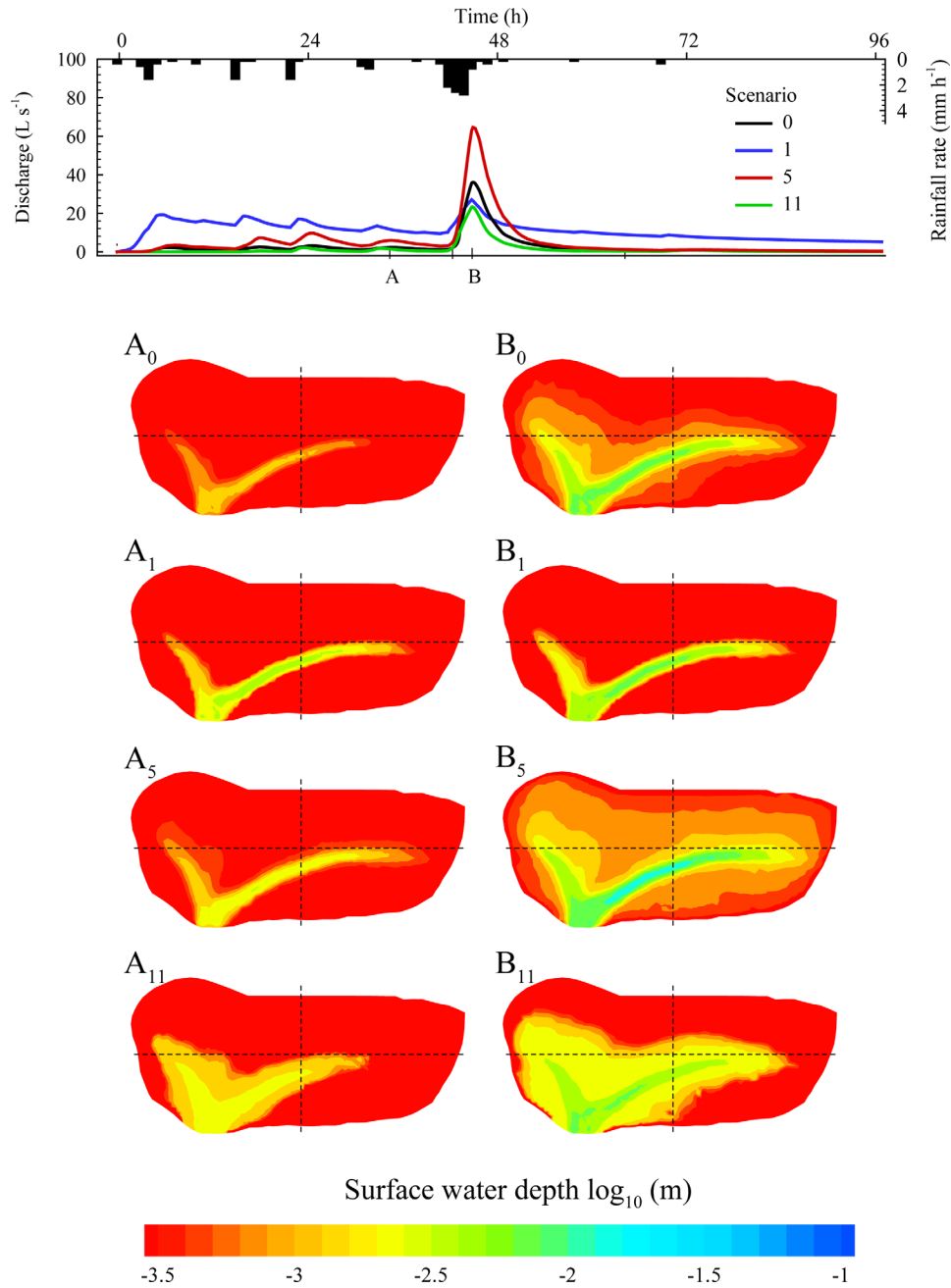


Figure 8. Simulated hydrologic response for TW Phase I, scenarios 0, 1, 5, and 11 (Table 2). The upper portion shows the event hyetograph and hydrographs of the integrated responses with two output times indicated (A and B). The lower portion shows snapshots of the distributed responses at the two output times. Snapshot A_0 is simulated output time A for TW-0. Dashed lines dividing the catchment into four quadrants are provided as a visual aid to assist in descriptions.

generally produce HOF (e.g., R5–28, Figure 10), with only a few notable exceptions. Even with rainfall intensities higher than the topsoil K_{sat} , in some Phase I scenarios (i.e., R5-4 and R5–16) the large available storage and high-infiltration gradients in the unsaturated near surface are sufficient to accommodate the small total rainfall depth (Table 3). Despite the dry initial conditions [see *Mirus et al.*, 2011a] the Dunne mechanism is also important for most R5 scenarios. Several alternative scenarios illustrate the relative importance DOF on the hydrologic response, which is controlled by the

permeability contrasts between the different soil units (e.g., R5–13 and R5–15, Figure 10).

[26] Figure 11 shows the subsurface hydraulic-head distribution during peak rainfall intensity for the base-case event (Figure 10, snapshot B_0). Examination of Figure 11 reveals the role of subsurface flow in hydrologic-response processes. The saturated zone above the wetting front extends with uniform thickness to the drainage divides (Figures 11b and 11c). The horizontal hydraulic-head gradient in the saturated topsoil/subsoil-1 (Figures 11b

MIRUS AND LOAGUE: HOW DOES RUNOFF BEGIN (AND END)?

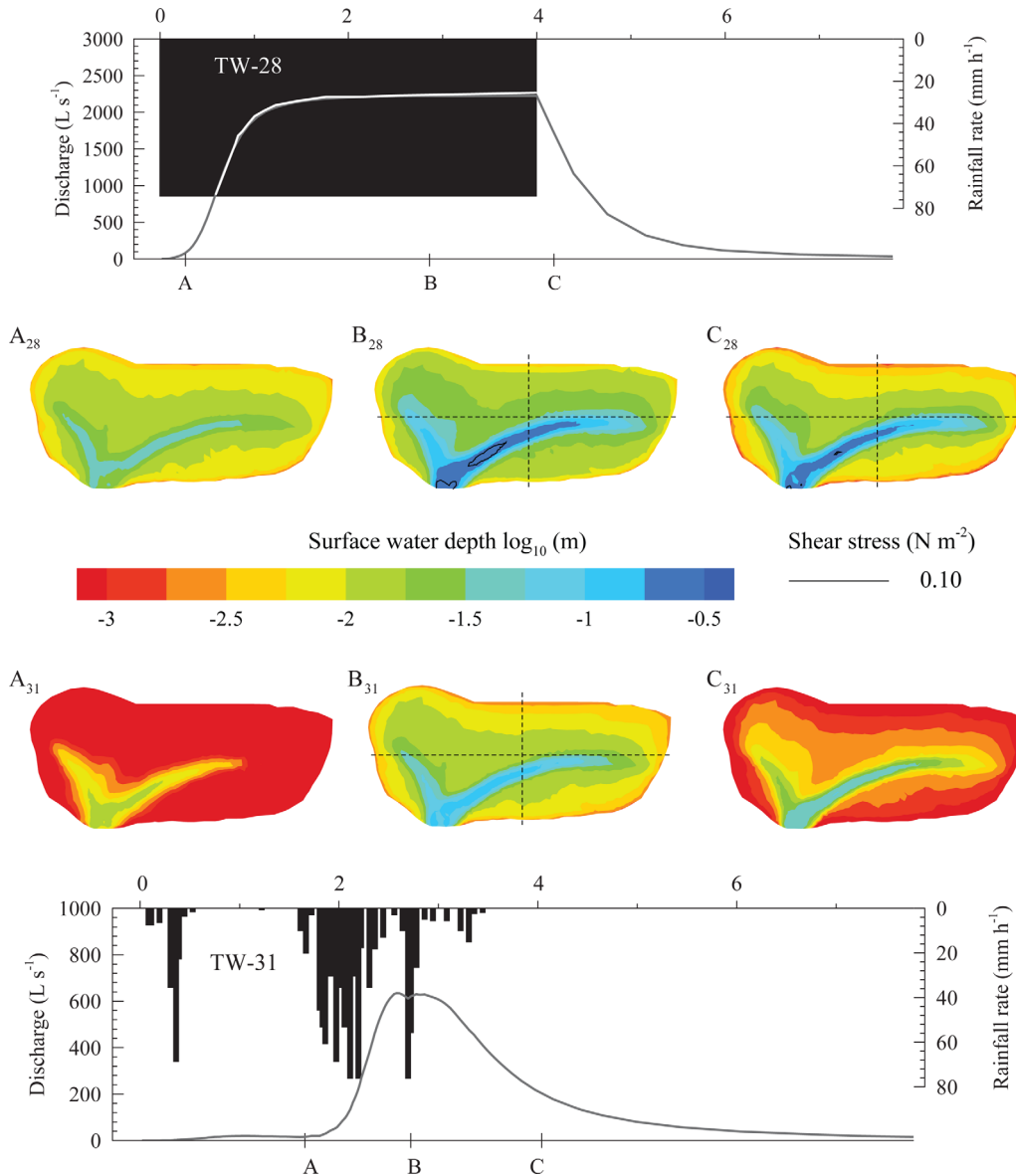


Figure 9. Simulated hydrologic response for TW Phase II, scenarios 28 (upper) and 31 (lower) (Table 3). Dashed lines dividing the catchment into four quadrants are provided as a visual aid to assist in descriptions.

and 11c) promotes lateral flow. The downward propagation of the wetting front is slowed by the permeability contrast between the subsoil-1 and subsoil-2 units. The predominantly vertical gradients in the unsaturated zone are punctuated by a sharp drop in hydraulic-head across the soil/bedrock interface (Figure 11), reflecting the more dramatic permeability contrast between the subsoil-2 and bedrock units. The deeper progression of the wetting front below the weir pond is impeded by the low-bedrock permeability, where a perched water table forms and promotes DOF in the area surrounding the weir pond (Figures 11b and 11c).

4.3. Controls on Runoff-Generation Processes

[27] The cumulative rainfall relative to the available unsaturated zone storage defines in large part the volume of SSSF draining laterally above the soil/bedrock interface. The distributed results show that SSSF velocities are

proportional to the hydraulic head gradient and saturated hydraulic conductivity of the soil units, but are not influenced by rainfall intensity. The permeability contrast between different hydrogeologic units, relative to the rainfall intensity is an important control on the hydrologic response. The volumetric flow rate of SSSF and the soil porosities control the height of the water table above the soil/bedrock interface. The water table rises and falls to accommodate the changes in volumetric flow rates that correspond to variations in rainfall intensity. The timing of expansion and contraction of the saturated contributing areas for SSSF are also controlled by the unsaturated hydraulic conductivities of the soil units and the rainfall intensities.

[28] The Dunne mechanism occurs when the saturated contributing area of SSSF expands to the point where the rising water table intersects the surface. The occurrence and extent of DOF is intimately coupled to the rate of SSSF

MIRUS AND LOAGUE: HOW DOES RUNOFF BEGIN (AND END)?

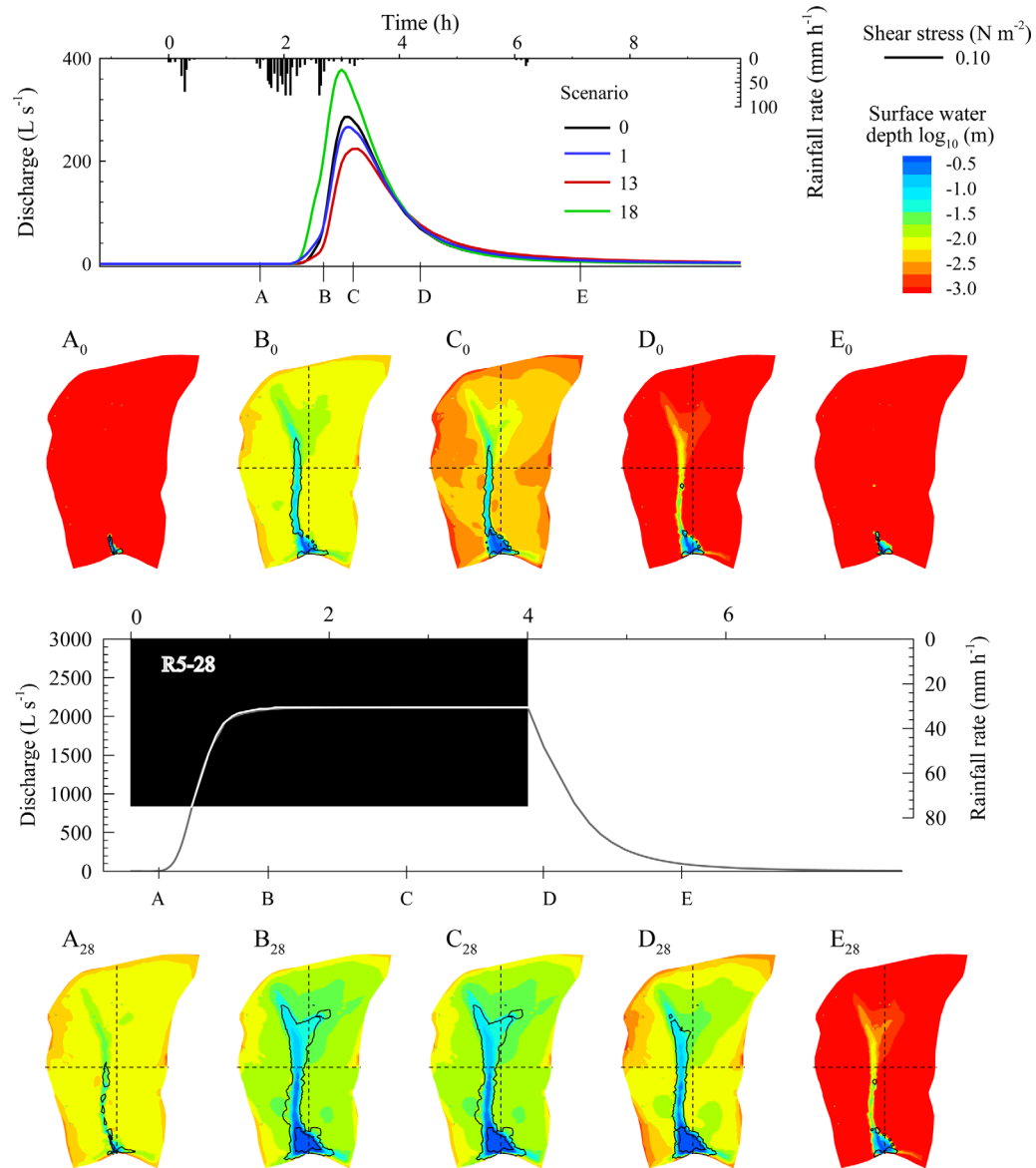


Figure 10. Simulated hydrologic response for R5 Phase I, scenarios 0, 1, 13, and 18 (see Table 2). The five output times (A through E) indicated on the hydrograph correspond to the snapshots of surface water depth and critical shear stress for the base case shown below. Snapshot A_0 is simulated output time A for R5-0.

relative to the cumulative rainfall input through time. Within breaks in slope, the elevation component of the hydraulic head gradient is decreased, leading to slower subsurface flow and a local rise in the water table. The rise of the water table is further accelerated within the topographic depression by the combination of slow groundwater discharge from the underlying bedrock and convergence of rapid SSSF from a large upslope contributing area. The topographic depression is always the starting (and ending) point of the variable source area for DOF.

[29] Once the combination of rainfall, overland flow, and exfiltration fill the unsaturated storage, runoff begins, which may infiltrate (as run-on) into the unsaturated subsurface down slope if conditions permit. Lateral expansion of the variable source area is promoted by lower permeability soil units, which limits the SSSF velocities and accelerates the

rise of the water table. Changes in the variable source area reflect the dynamics of the water table, which rises in response to sustained rainfall at intensities greater than the saturated hydraulic conductivity of the bedrock. Although the soil porosity and shape of the characteristic curves influence the timing of both subsurface flow and DOF, they do not impact the overall runoff patterns as strongly as the saturated hydraulic conductivity and rainfall characteristics (average intensity and total depth), particularly on steeper slopes like C3 and CB.

[30] Surface runoff begins and ends within topographic depressions and convergent topography, regardless of whether HOF or DOF is dominant. For smaller events of low- to moderate-rainfall intensity and/or total depth, the rise in the water table is sufficiently low that DOF re-infiltrates into the unsaturated soils just down-gradient from the

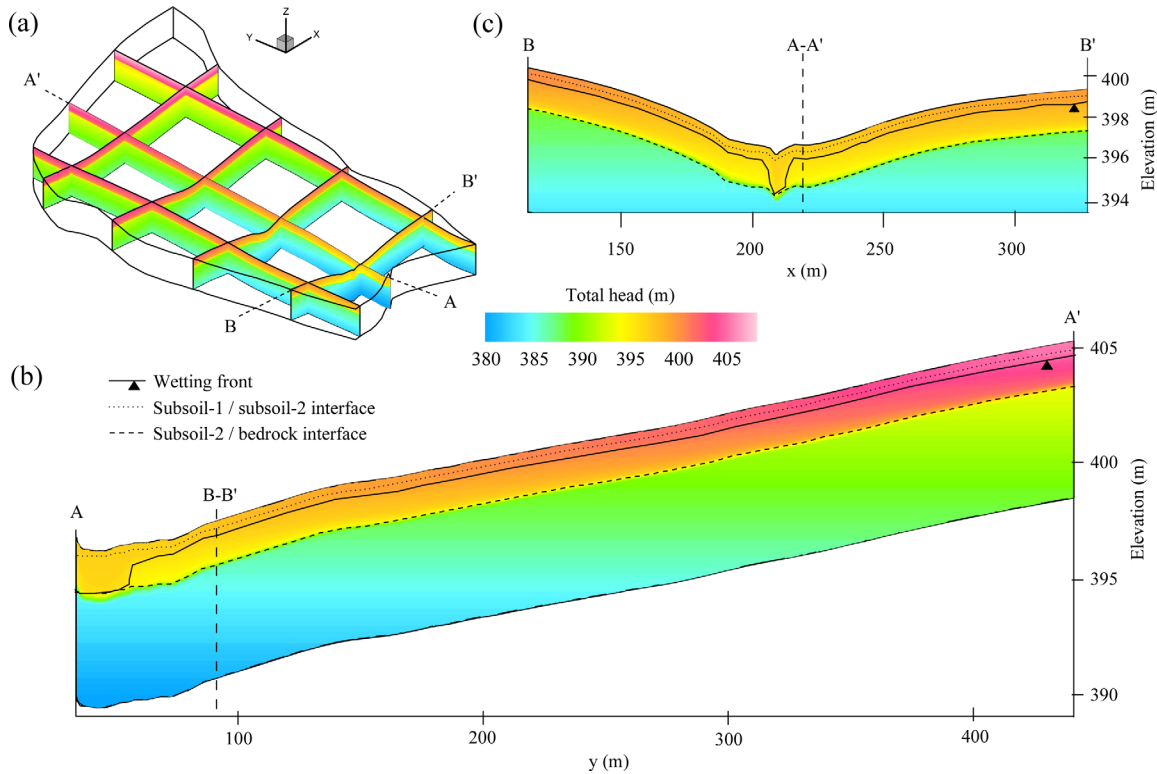


Figure 11. Subsurface hydraulic head distribution for the R5 base case at output time B (see Figure 10, snapshot B₀). (a) 3-D fence diagram of the entire catchment. (b) 2-D slice for the A-A' transect. (c) 2-D slice for the B-B' transect.

topographic depression, contributing to the integrated response as SSSF. When surface runoff flows continuously between the topographic depression and the catchment outlet it contributes directly to the integrated response. This occurs when either rainfall intensities exceed the surface saturated hydraulic conductivity or sustained rainfall (of moderate to high intensity) results in the volumetric flux of SSSF that greatly exceeds the storage capacity of high-permeability soil layers.

[31] The relative contribution of HOF and DOF is controlled by the hydraulic properties of all soil units. When rainfall intensities exceed the saturated hydraulic conductivity of the topsoil unit (see Tables 1–3), HOF occurs, provided there has been sufficient rainfall depth to fill the near surface storage and generate ponding. Under dry initial conditions, the water-retention curve strongly controls the unsaturated zone storage for the initial pressure head distribution, thereby dictating the rainfall depth required to induce ponding at the surface (e.g., compare scenarios R5-0 and R5-4). Since the hydrogeologic units in this study are uniform, when HOF does occur, overland flow is generated throughout the catchment of interest. For a given hydrogeologic unit, the characteristic curves influence the factors governing the rate of wetting front propagation, including: (i) unsaturated hydraulic conductivity, (ii) hydraulic-head gradient, and (iii) volume of unsaturated zone storage available. Wetting front velocity controls the partitioning between infiltration and HOF. Upon reaching an interface between hydrogeologic units, the wetting front propagation and infiltration rates at the surface adjust to

accommodate the hydraulic properties of the underlying unit. Flow paths through the overlying saturated unit shift toward the slope-parallel direction in proportion to the permeability contrast with the underlying unit. The overlying unit remains saturated as long as rainfall continues at rates greater than the leakage into the underlying unit.

[32] Under wet initial conditions, unsaturated zone storage is minimal and the influence of the characteristic curves and surface K_{sat} is limited. Instead K_{sat} of subsoil layers affects the relative rates of lateral subsurface flow through the saturated hydrogeologic units. When HOF does occur, the downwardly propagating wetting front quickly reaches the water table and the entire soil column becomes saturated, resulting in overland flow that according to traditional classification could be categorized as either HOF or DOF. For low-gradient topography, subsurface drainage is slow, and runoff response and water table dynamics are both proportional to variations in rainfall intensity.

4.4. Developing a Quantitative Dunne-Like Diagram

[33] The investigations of individual soil-hydraulic properties in Phase I and rainfall characteristics in Phase II consider a range of environmental conditions (Figure 1) and employ realistic topographies (Figure 2). The hydrologic response processes gleaned from these concept-development simulations with multiple hydrogeologic layers provide insights into how runoff is generated. In particular, the results herein show that topsoil K_{sat} and rainfall intensity are not the only controls on how runoff begins (and ends). Indeed several alternative simulation scenarios demonstrate

the importance of total rainfall depth, hydraulic properties of the subsoil units, and unsaturated zone storage characteristics on the initiation and cessation of surface runoff. The system variables can, in general, be divided into two groups: (i) those that influence the rates of flow, and (ii) those that control the available unsaturated zone storage. Because the hydrologic response of each system is dynamic, the storage volume through time is intrinsically linked to the rates of flow. The emergent behavior for each simulation scenario reflects the coupling between rates of flow and changes in storage. A comprehensive quantitative representation of the Dunne diagram should represent the effects of both these factors.

[34] Figure 1 is inverted from the original format of the diagram [see *Dunne*, 1978] to facilitate adding quantitative axes and identifying process thresholds. Figure 1 provides a template for quantitatively cataloguing the alternative scenarios based on their parameterizations and simulated runoff-generation mechanisms. Figure 12 is a quantitative Dunne-like diagram with dimensionless terms for rates of flow and storage. On the x -axis, the rate term is the ratio of event-averaged rainfall intensity to the surface saturated hydraulic conductivity, similar to the r^* used by *Smith and Hebbert* [1983]. On the y -axis, the storage term is the ratio of cumulative depth of the rainfall event to the depth equivalent of the initial unsaturated storage prior to the rainfall event, which is similar to the concept of drainable porosity [e.g., *Weiler and McDonnell*, 2004]. The simple metric for unsaturated zone storage, applied consistently for all scenarios, calculates the initial volume of unsaturated pores above the soil/bedrock interface in the area of the catchment midpoint (defined using the four quadrants shown in Figures 5 through 10). These rate and storage metrics are employed because they are calculated with information that can not only be gleaned from a simulation, but also could be measured directly in the field.

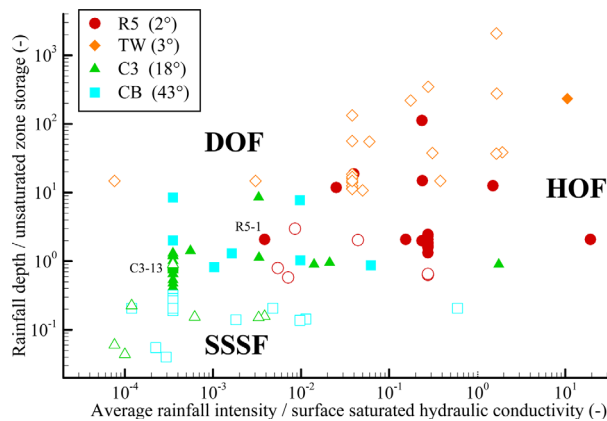


Figure 12. Summary of simulation results for the 140 Phase I and II scenarios using nondimensional ratios for infiltration and storage. Closed and open symbols indicate the occurrence and absence of surface runoff, respectively (see Tables 2 and 3). The average slope along the catchment hollows are given in brackets for each catchment. Streamflow generation mechanisms are shown as end members: Horton overland flow (HOF), Dunne overland flow (DOF), and subsurface stormflow (SSSF). Selected scenarios C3-13 and R5-1 are labeled.

[35] The differences between the four base-case BVPs and their corresponding alternative scenarios are reflected by the variations in the values of the rate/storage ratios for the simulations where surface runoff occurs. Figure 12 groups the scenarios in terms of the four base-case topographies, which provides a starting point for discussion. Within each group of scenarios derived from the different catchments there is a general trend that surface runoff occurs for the higher values of the rates and storage ratios, which is expected. However, some further insights are possible through examining the differences between the four catchments as well as explaining some notable exceptions to the trends, which are the subjects of the remainder of this section.

[36] The dimensionless format of Figure 12 facilitates incorporating the important effects of the soil-hydraulic properties, rainfall characteristics, and initial conditions considered in this study into a unified quantitative framework that is not possible in Figure 1. For instance, the impact of porosity, residual saturation, and the characteristic curves on unsaturated zone storage are reflected by the vertically aligned cluster of scenarios around each base case. Gently sloping characteristic curves, high-residual soil-water content, low porosity, and wet initial conditions all decrease unsaturated zone storage. As quantitatively illustrated by the R5 and CB scenarios, minimal changes in the storage ratio can be sufficient to cross the threshold for overland flow via either the Horton or Dunne mechanism.

[37] The complexity of characterizing surface runoff thresholds with Figure 12 increases when comparing scenarios with different topographies to one another. The well-known importance of topography on driving subsurface water flow [*Beven and Kirkby*, 1979] is somewhat confounded by the different subsurface layers, hydraulic properties, and rainfall characteristics for each set of alternative scenarios (Tables 1 and 3). However, the four topographies (Figure 2) span the range of possible slope angles in soil-mantled landscapes. Despite the unique hydrogeologic parameterizations and topographies of the four base-case BVPs, some generalized insights can be gleaned from a cross comparison of Figures 1 and 12. For the C3 and CB scenarios, surface runoff occurs over a similar range of low values for the rate (~ 0.0005 – 2.0) and storage ratios (~ 0.5 – 10.0). For the R5 scenarios, relative to the C3 and CB scenarios, surface runoff generally occurs for slightly higher rate (> 1.0) and storage ratios (~ 0.03 – 20.0). For the TW scenarios, surface runoff occurs only when rate (10.5) and storage (233.0) ratios are orders of magnitude higher than for the C3, R5, and CB scenarios.

[38] The similarity between the surface runoff thresholds for the C3 and CB scenarios (Figure 12) quantitatively confirms that hydrologic response for steep slopes with developed soil profiles (Table 1) is strongly influenced by the topography and the rainfall depth relative to the unsaturated zone storage. Conversely, the contrast between the runoff thresholds for TW and R5 scenarios (Figure 12) quantitatively confirms that for gently sloping topography the soil-hydraulic properties and rainfall characteristics define a more delicate balance of hydrologic-response processes. It should be pointed out that both TW and R5 have similar drainage areas and average slopes. Despite the range of rainfall conditions and soil-hydraulic properties considered

in Phases I and II, the R5 scenarios generally produce surface runoff while the TW scenarios do not. This unexpected result is despite the wetter initial conditions [Mirus *et al.*, 2011a] employed for TW relative to the thick unsaturated zone for R5.

[39] The impact of the hydraulic properties for the contrasting subsurface layers simulated in Phases I and II demonstrate how the TW and R5 scenarios differ in terms of the subsurface drainage dynamics. Characteristics of the topography, such as the degree of hillslope curvature, the catchment length to width ratio, and boundary conditions explain some of the differences in runoff patterns between the R5 and TW scenarios. However, the primary difference between the surface runoff thresholds for the R5 and TW BVPs is related to the influence of contrasting surface roughness values employed for the two catchments [see Mirus *et al.*, 2011a]. Surface roughness has a moderate impact on the discharge hydrograph and a substantial impact on the critical shear stress calculations, but is beyond the scope of this study.

[40] Two notable exceptions to the general pattern gleaned from Figure 12 are scenarios C3-13 and R5-1. While the value of the rate ratio for C3-4 through C3-24 is the same, only C3-13 does not produce DOF. As illustrated in Figure 4 and described above (see section 4.2.1.1.), the highly permeable subsoil-1 unit for C3-13 facilitates rapid lateral drainage of SSSF, eliminating the Dunne mechanism. Saturated hydraulic conductivity of the subsurface layers is not explicitly incorporated into the dimensionless rate ratio, explaining why C3-13 appears as an outlier in Figure 12. Comparison of R5-1 with neighboring scenarios in Figure 12 further highlights the importance of subsoil permeability on runoff response. For example, R5-30 and R5-32 were generated by assigning alternative rainfall events with lower peak and average intensities (Table 3) and did not yield surface runoff, whereas R5-1 was generated by increasing the topsoil saturated hydraulic conductivity (Table 2), which did yield surface runoff. For R5, decreasing the rainfall intensity eliminates HOF and surface runoff, whereas increasing the saturated hydraulic conductivity of the topsoil merely shifts the runoff generation mechanism from partial HOF to purely DOF and the runoff pattern remains largely unchanged [see Mirus, 2009]. The low-saturated hydraulic conductivity of the subsoil-1 unit relative to the base-case rainfall intensity promotes rapid rise of perched water at the topsoil/subsoil-1 interface, which saturates the highly permeable topsoil and leads to DOF.

[41] The C3-13 and R5-1 scenarios provide examples of how the simulations quantitatively identified the hydraulic conductivity of the subsoil-1 unit as an important control on the occurrence of overland flow for both steep and gently sloping topography. Further examination of results for the other C3 scenarios revealed that upward hydraulic gradients across the soil-bedrock interface in the region underlying the topographic depression contributed to the occurrence of DOF (see Figure 7). In contrast, the R5 scenarios all displayed uniformly downward head gradients along the soil-bedrock interface below the weir pond (see Figure 11), which did not substantially impact the runoff response. Future iterations of the quantitative Dunne diagram in Figure 12 could develop a rates ratio to accommodate the

influence of the subsoil and bedrock head gradients on overland flow generation.

[42] Overall, Figure 12 illustrates how the parameter space and topographies considered in this study leads to a wide range of possible runoff responses. It is furthermore clear that the simulations plotted in Figure 12 merely scratch the surface of a virtually infinite spectrum of possible alternative scenarios. For natural systems over the time scale of single rainfall-runoff events, temporal variations in soil-hydraulic properties are minimal compared to the dynamic variability of initial storage and rainfall intensities/duration. The formulation of the Dunne-like diagram presented in Figure 12 is particularly useful for examining the influence of rainfall characteristics on runoff thresholds for a given location and for comparison between different locations.

5. Discussion

[43] The work presented herein is a simulation-based effort to investigate the spatial patterns of runoff generation dynamics for multiple complex topographies (Figure 2) and soil layer configurations (Table 1) with a range of characteristics curve shapes (Figure 3). In contrast to previous virtual experiments [Freeze, 1980; Weiler and McDonnell, 2004], InHM represents the fully coupled physics of surface and subsurface flow in multiple dimensions. Unlike many applications of hydrologic models comparable to InHM, the original BVPs that form the foundation for this study were rigorously evaluated with rich data sets of both integrated and distributed hydrologic response [Ebel *et al.*, 2007b; Heppner *et al.*, 2007; Mirus *et al.*, 2007, 2009a]. Therefore, if one accepts the validity of the physics upon which InHM is built [VanderKwaak, 1999; VanderKwaak and Loague, 2001], the quality of the data collected for each experimental catchment [Dutton *et al.*, 2005; Ebel *et al.*, 2007a; Heppner and Loague, 2008; Western and Grayson, 1998], and the minimal simplifications made in the developing the base-case BVPs [Mirus *et al.*, 2011a], then the alternative simulation scenarios can be taken as individual hypothetical realities [e.g., Mirus *et al.*, 2011b]. The quantitative comparison of these hypothetical realities provides novel insights into the interactions that influence runoff-generation processes.

[44] The simulation results demonstrate that for the physically realistic parameter space defined by the base-case BVPs, the entire spectrum of streamflow generation mechanisms is possible. The wide ranges of rainfall duration/intensity and saturated hydraulic conductivity/water retention properties in this study correspond to high variability in unsaturated zone storage and subsurface flow rates, comparable to those observed in natural systems [e.g., Dunne, 1978]. The overlap between the characteristics promoting both the Horton and Dunne mechanisms supports the assessments of Freeze [1972a, 1972b], Smith and Hebbert [1983], and Loague *et al.* [2010], that the two mechanisms of overland flow generation represent end-members of a continuum of subsurface controlled rainfall-runoff processes. Conversely, the results herein demonstrate that SSSF and DOF are two competing mechanisms. Thus, while the traditional conceptual classification of streamflow generation mechanisms (Figure 1) is supported

by the simulation results, it is clear that quantitatively characterizing the dynamics of rainfall-runoff processes is more complex (Figure 12). The results demonstrate how individual mechanisms may dominate the discharge hydrographs, whereas the distributed runoff response often reflects a combination of runoff generation processes that are critical for establishing streamflow.

[45] The results quantitatively confirm findings from previous studies that saturated hydraulic conductivity is the parameter with the strongest influence on runoff generation [e.g., Freeze, 1980; Smith and Hebbert, 1983; Loague, 1988; Binley *et al.*, 1989a, 1989b]. In contrast, porosity, residual saturation, and the characteristic curves have a narrower, yet important influence on the available storage in the unsaturated zone and, subsequently, surface runoff response. The results also quantitatively confirm the importance of topography on surface runoff [Horton, 1945; Smith and Bretherton, 1972; Montgomery and Dietrich, 1989]. Hillslope gradients exert a very strong control on lateral drainage through permeable soil layers, so topographic convergence and average slope influence the transition between SSSF- and DOF-dominated responses.

5.1. Unsaturated Storage Dynamics

[46] While the variability in rainfall and saturated hydraulic conductivity provide the primary controls on the thresholds between the Horton and Dunne mechanisms, for gently sloping topography the characteristic curves set a delicate balance for the occurrence of overland flow by either mechanism. The relative contributions of HOF and DOF were shown to strongly influence the timing and magnitude of peak runoff as well as the distributed runoff patterns. The nonlinearity of the characteristic curves results in unsaturated hydraulic conductivity variations over several orders of magnitude (see Figure 3). The distributed simulation results demonstrate how the unsaturated hydraulic conductivity of the topsoil layer controls: (i) infiltration rates, which are related to the occurrence of ponding and the onset of HOF; (ii) timing and magnitude of the saturated volume contributing to SSSF; and (iii) variable source area dynamics for DOF. Although this study considers only individual rainfall-runoff events, continuous simulations for TW have been used to demonstrate how uncertainty associated with estimating characteristic curves can propagate through time [Mirus *et al.*, 2011c].

5.2. Soil Layers and Permeability Contrasts

[47] The soil-water retention and unsaturated hydraulic conductivity curves for the subsoil layers also play an important role in water table fluctuations and saturation thresholds, particularly when the unsaturated zone extends below the interface between units with contrasting hydraulic properties. The effect of permeability contrasts between unsaturated units can be enhanced or muted depending on the characteristics curve shapes. For example, given two soil layers with the same characteristic curve shapes and a higher saturated hydraulic conductivity in the overlying unit, the permeability contrast with the underlying unit is increased when the soil column wets from above. Increases in the permeability contrasts between unsaturated hydrogeologic units are the greatest for low-saturated hydraulic conductivities (e.g., bedrock), since greater head gradients

are required to drive fluxes across the interface between less permeable units. These unsaturated flow dynamics generally promote perched water table development and the occurrence of DOF, as demonstrated by most of the alternative simulation scenarios for R5.

[48] This study quantitatively confirms previous speculations that multiple soil layers greatly complicate “*the probabilistic interactions of rainfall distribution and soil property distributions*” [Smith and Hebbert, 1983]. The concept-development simulations reported herein indicate that even homogeneous soil layers provide critical controls on the threshold-like behavior of runoff generation. The strong impact of multiple permeability contrasts on wetting front and lateral flow velocities underscores the motivation of recent efforts to estimate effective anisotropies for variably saturated systems [e.g., Yeh *et al.*, 2005; Vereecken *et al.*, 2007; Mirus *et al.*, 2009b]. In general, the importance of the subsoil units on the range of streamflow generation mechanisms indicates that regardless of climate and topography, an assessment of soil stratigraphy, not just soil thickness, should be a prerequisite for any rigorous characterization of hydrologic-response dynamics.

5.3. Topography and Surface/Subsurface Flow Convergence

[49] Lateral convergence of subsurface flow above a permeability contrast generally leads to the initial onset of DOF by accelerating the rise of a perched or local water table. Accumulation of HOF in convergent topography provides elevated hydraulic head gradients, which drives continuous infiltration and enhanced wetting-front propagation. HOF may thereby promote the development of a variable source area for DOF, localized within even very gently convergent topography. Pure HOF would therefore be restricted to environments with thick, homogeneous soils, a deep water table, and sustained high-intensity rainfall. Freeze [1980] remarked with wonder upon the narrow range of topographic, climatic and soil conditions for which the Dunne mechanism occurred within the confines of his stochastic-conceptual simulations. In contrast, the results from this study indicate that the Dunne mechanism is active over a wide range of average slopes, rainfall intensities, and soil-hydraulic properties, due to soil layering and topographic convergence. The importance of convergent subsurface flow has indeed long been recognized [e.g., Freeze, 1972a, 1972b; Beven, 1977; Smith and Hebbert, 1983; Dunne, 1990] and was quantitatively demonstrated with InHM by Mirus *et al.* [2007].

[50] Distributed results show that regardless of the dominant streamflow-generation mechanism, topographically enclosed areas act as a seed for the beginning (and ending) of runoff by the Dunne mechanism. Exfiltration and rapid runoff on the abrupt topographic features such as the C3 road-cut and the R5 weir/pond provide examples of how anthropogenic changes in topography affect the dynamics of the coupled groundwater/surface water flow systems. This serves as a healthy reminder of the *observer effect*, notably that through measuring a hydrologic system variable (e.g., discharge measured by a v-notch weir at R5), the system response is itself altered. It is worth noting that the development of the TW base case intentionally omitted the expression of the roads and weir, to produce a more generic

hypothetical reality of hydrologic response [Mirus *et al.*, 2009a, 2011b].

[51] The complex influences of average and local slopes with topographic convergence and curvature gleaned from the simulation results demonstrates that the scope of this study is heavily influenced by the selection of the four base-case topographies (Figure 2). Figure 12 shows that the widely acknowledged impact of topographic slope is reflected by the contrast in surface runoff response between the steeply sloping catchments (i.e., C3 and CB) compared to the gentler sloping catchments (i.e., TW and R5). Additional alternative scenarios representing a greater range of simple and complex topography are possible, but are unlikely to lead to greater insights beyond the general trends shown in Figure 12. Using simulations with generic topographies that span the gaps between the four base cases could facilitate adding a z -axis to Figure 12. The results from this study suggest that despite the well-known influence of gravity on driving hillslope hydrologic response, topography must be considered in combination with the subsurface geometry and hydraulic properties to capture the important influence of flow convergence.

6. Perspectives and Conclusions

[52] Runoff generation is inherently a problem of relative rates between infiltration and changes in near-surface storage, which is reasonably well captured for a given catchment using the quantitative Dunne-like diagram (Figure 12). The dimensionless rate and storage ratios proposed in Figure 12 are not completely unique, nor is the critical shear stress concept used to define surface runoff in this study without simplifications. However, their combination in a two-dimensional format inspired by the original Dunne diagram (Figure 1) provides a novel means for cataloguing concept-development simulations and also quantitatively assessing the controls on runoff generation in real catchments. The results from alternative simulation scenarios in this study demonstrate the type of surface/subsurface water interactions associated with the different runoff generation mechanisms. Some scenarios produced similar integrated responses, though not necessarily the same distributed runoff dynamics. Additionally, some of the scenarios that respond with a combination of DOF and SSSF display similar runoff patterns and rather different integrated responses. The delicate balance between the factors that favor one runoff generation mechanism over another is further complicated by the observation that for layered soils, topographic convergence of HOF and SSSF alike promote the initiation of DOF.

[53] Only in extreme cases do individual runoff-generation mechanisms act in isolation, particularly for the HOF mechanism. Whereas the Horton and Dunne mechanisms represent a complex continuum of processes resulting in overland flow, SSSF and the Dunne mechanism are shown to be competing hydrologic processes that can occur simultaneously. This insight could be tangentially related to geomorphic process thresholds [Dietrich and Dunne, 1993; Dietrich *et al.*, 2003], such as the transition from landscapes dominated by shallow landslides (where detached sediment is evacuated infrequently by mass wasting) to persistent stream channels (where detached sediment is

regularly removed by overland flow). The frequent occurrence of multiple runoff-generation mechanisms for a single alternative simulation scenario suggests that single-process models (e.g., HOF) cannot always adequately represent observed hydrologic response. For the wide range of scenarios in this study, the relative contributions of the different runoff generation mechanisms are defined by a delicate balance of very dynamic processes.

[54] Topographic convergence promotes lateral drainage within the variably saturated soil layers, which is important regardless of the dominant runoff-generation mechanisms, because it feeds the development of a variable source area for DOF. Thus for homogeneous soil layering, DOF begins (and ends) within the most convergent topography, not necessarily in the region with the greatest upslope contributing area. On very steep slopes, large gravitational components to the hydraulic head gradient drive rapid lateral drainage that overshadows the impacts of soil-hydraulic properties, thereby promoting SSSF instead of overland flow. The simulation results herein suggest that geomorphic process thresholds such as the transition from stream channels up into landslide dominated hillslopes [Stock and Dietrich, 2003] can be related in part to environmental conditions favoring DOF and SSSF, respectively.

[55] Compared to the difficulty of mapping surface saturation in the field for a single site [e.g., Dunne and Black, 1970a, 1970b], the relative ease with which InHM simulated output provides temporally exhaustive runoff patterns for multiple events and topographies underscores the utility of hypothetical-reality data sets and concept-development simulations. However, the intricate nature of evaluating the simulated output for each alternative scenario summarized in Tables 2 and 3, and Figure 12 is perhaps somewhat underemphasized [Mirus, 2009]. Regardless, the complex influence of soil layering and hydraulic properties under variable rainfall conditions is difficult to tease out of observations from individual field sites or to predict for locations where no measurements are present. The quantitative framework developed herein for addressing the question of how runoff begins (and ends) provides useful insights into future heuristic applications of InHM. For instance, an automatic mesh generation algorithm would facilitate the consideration of alternative topographies with incremental variations in slope and curvature to assess the impact of erosion processes and engineered structures.

[56] The motivation for this research was to carefully characterize the hydrology associated with runoff generation in first-order catchments. The importance of large events in generating runoff and sculpting landscapes underscores the utility for an improved physical understanding of the conditions that promote or deter the occurrence of surface runoff over a range of environments. It is demonstrated herein that comprehensive assessment of transient, multidimensional, variably saturated flow processes are essential to developing simplified representations of hydrologic response. The central role of lateral flow within the near-surface soil layers for both steeply and gently sloping topographies suggests that incorporating hydrologic response into models of soil formation would provide useful insights into the causes and effects of stratification inherent to hillslope networks. In a concept-development mode, physics-based simulation could provide a practical

framework for further examination of how variable water fluxes are accommodated in different soil-mantled environments over a range of spatial and temporal scales for both real and hypothetical topographies.

[57] **Acknowledgments.** This work was supported in part by the Stanford UPS Endowment Fund. The first author is grateful for a Stanford Graduate Fellowship. We greatly appreciate the lively discussions with Brian Ebel, Chris Heppner, and Joel VanderKwaak on the topic of runoff generation. Thanks to Kevin Schmidt and three anonymous reviewers, who provided useful suggestions that helped improve this manuscript.

References

- Beven, K. J. (1977), Hillslope hydrographs by the finite-element method, *Earth Surf. Process.*, 2, 13–28.
- Beven, K. J. (1997), TOPMODEL: A critique, *Hydrol. Process.*, 11, 1069–1085.
- Beven, K. J. (2006), Streamflow generation, in *IAHS Benchmark Papers in Hydrology*, edited by J. J. McDonnell, vol. 1, 432 p., IAHS Press, Wallingford, U. K.
- Beven, K. J., and M. J. Kirkby (1979), A physically based, variable contributing area model of basin hydrology, *Hydrol. Sci.*, 24, 1–3.
- Binley, A. M., J. Elgy, and K. J. Beven (1989a), A physically-based model of heterogeneous hillslopes I. Runoff production, *Water Resour. Res.*, 25, 1219–1226.
- Binley, A. M., K. J. Beven, and J. Elgy (1989b), A physically-based model of heterogeneous hillslopes II. Effective hydraulic conductivities, *Water Resour. Res.*, 25, 1227–1233.
- Dietrich, W. E., and T. Dunne (1993), The channel head. In *Channel Network Hydrology*, edited by J. K. Beven and M. J. Kirkby, pp. 175–219, John Wiley, New York.
- Dietrich, W. E., D. Bellugi, A. M. Heimsath, J. J. Roering, L. Sklar, and J. D. Stock (2003), Geomorphic transport laws for predicting the form and evolution of landscapes, in Wilcock, P. R., and R. M. Iverson (Eds.) (2003), *Prediction in Geomorphology, Geophys. Monogr. Ser.*, vol. 135, 256 pp., AGU, Washington, D. C., doi:10.1029/GM135.
- Dunne, T. (1978), Field studies of hillslope flow processes, in *Hillslope Hydrology*, edited by M. J. Kirkby, pp. 227–293, John Wiley, New York.
- Dunne, T. (1990), Hydrology, mechanics and geomorphic implications of erosion by subsurface flow, in *Ground Water Geomorphology: The Role of Subsurface Water in Earth-Surface Processes and Landforms, Geol. Soc. of Am. Special Pap.* 252, pp. 1–28, edited by C. G. Higgins and D. R. Coates, GSA, Boulder, Colo.
- Dunne, T., and R. G. Black (1970a), An experimental investigation of runoff production in permeable soils, *Water Resour. Res.*, 6, 478–490.
- Dunne, T., and R. G. Black (1970b), Partial area contributions to storm runoff in a small New England watershed, *Water Resour. Res.*, 6, 1296–1311.
- Dutton, A. L., K. Loague, and B. C. Wemple (2005), Simulated effect of a forest road on near-surface hydrologic response and slope stability, *Earth Surf. Process. Landforms*, 30, 325–338.
- Ebel, B. A., K. Loague, W. E. Dietrich, D. R. Montgomery, R. Torres, S. P. Anderson, and T. W. Giambelluca (2007a), Near-surface hydrologic response for a steep, unchanneled catchment near Coos Bay, Oregon: 1. Sprinkling experiments, *Am. J. Sci.*, 307, 678–708, doi:10.2475/04.2007.02.
- Ebel, B. A., K. Loague, J. E. VanderKwaak, W. E. Dietrich, D. R. Montgomery, R. Torres, and S. P. Anderson (2007b), Near-surface hydrologic response for a steep, unchanneled catchment near Coos Bay, Oregon: 2. Physics-based simulations, *Am. J. Sci.*, 307, 709–748, doi:10.2475/04.2007.03.
- Freeze, R. A. (1972a), Role of subsurface flow in generating surface runoff 1. Base flow contributions to channel flow, *Water Resour. Res.*, 8, 609–624.
- Freeze, R. A. (1972b), Role of subsurface flow in generating surface runoff 2. Upstream source areas, *Water Resour. Res.*, 8, 1272–1283.
- Freeze, R. A. (1980), A stochastic-conceptual analysis of rainfall-runoff processes on a hillslope, *Water Resour. Res.*, 16, 391–408.
- Heppner, C. S., and K. Loague (2008), Characterizing long-term hydrologic-response and sediment-transport for the R-5 catchment, *J. Environ. Qual.*, 37, 2181–2191.
- Heppner, C. S., K. Loague, and J. E. VanderKwaak (2007), Long-term InHM simulations of hydrologic response and sediment transport for the R-5 catchment, *Earth Surf. Process. Landforms*, 32, 1273–1292.
- Horton, R. E. (1945), Erosional development of streams and their drainage basins; hydrophysical approach to quantitative morphology, *Geol. Soc. Am. Bull.*, 56, 275–370.
- Loague, K. (1988), Impact of rainfall and soil hydraulic property information on runoff predictions at the hillslope scale, *Water Resour. Res.*, 24, 1501–1510.
- Loague, K. (2010), Rainfall-runoff modeling, in *IAHS Benchmark Papers in Hydrology*, edited by J. J. McDonnell, vol. 4, 506 p., IAHS Press, Wallingford, U. K.
- Loague, K., C. S. Heppner, B. B. Mirus, B. A. Ebel, Q. Ran, A. E. Carr, S. H. BeVile, and J. E. VanderKwaak (2006), Physics-based hydrologic-response simulation: Foundation for hydroecology and hydrogeomorphology, *Hydrol. Process.*, 20, 1231–1237.
- Loague, K., C. S. Heppner, B. A. Ebel, and J. E. VanderKwaak (2010), the quixotic search for a comprehensive understanding of hydrologic response at the surface: Horton, Dunne, *Dunton*, and the role of concept-development simulations, *Hydrol. Process.*, 24, 2499–2505, doi:10.1002/hyp.7834.
- Mirus, B. B. (2009), How does runoff begin (and end)? Ph.D. dissertation, 288 pp., Stanford Univ., Stanford, Calif.
- Mirus, B. B., B. A. Ebel, K. Loague, and B. C. Wemple (2007), Simulated effect of a Forest Road on near-surface hydrologic response: Redux, *Earth Surf. Process. Landforms*, 32, 126–142, doi:10.1002/esp.1387.
- Mirus, B. B., K. Loague, J. E. VanderKwaak, S. Kampf, and S. J. Burges (2009a), A hypothetical reality of Tarrawarra-like hydrologic response, *Hydrol. Process.*, 23, 1093–1103, doi:10.1002/hyp.7241.
- Mirus, B. B., K. Perkins, J. R. Nimmo, and K. Singha (2009b), Hydrologic characterization of desert soils with varying degrees of pedogenesis: II. Inverse modeling for effective properties, *Vadose Zone J.*, 8, 496–509, doi:10.2136/vzj.2008.0051.
- Mirus, B. B., B. A. Ebel, C. S. Heppner, and K. Loague (2011a), Assessing the detail needed to capture rainfall-runoff dynamics with physics-based hydrologic-response simulation. *Water Resour. Res.*, 47, W00H10, doi:10.1029/2010WR009906.
- Mirus, B. B., K. Loague, N. C. Cristea, S. J. Burges, and S. K. Kampf (2011b), A synthetic hydrologic-response dataset. *Hydrol. Process.*, 25, 3688–3692, doi:10.1002/hyp.8185.
- Mirus, B. B., J. R. Nimmo, and K. Loague (2011c), The influence of scale and structure on soil-hydraulic property estimates: Implications for modeling surface and near-surface hydrology, paper presented at SSSA Annual Meeting, San Antonio, TX, Abstract 341-7.
- Montgomery, D. R., and W. E. Dietrich (1989), Source areas, drainage density, and channel initiation, *Water Resour. Res.*, 25, 1907–1918.
- Ritter, D. F., R. C. Kochel, and J. R. Miller (1978), *Process Geomorphology*, pp. 560, McGraw-Hill, New York, N. Y.
- Shields, A. (1936), *Anwendung der Ähnlichkeits-Mechanik und der Turbulenz-forschung auf die Geschiebebewegung*, Preussische Versuchsanstalt für Wasserbau und Schiffbau, vol. 26, Triltsch & Huther, Berlin, Germany.
- Sidle, R. C., and Y. Onda (2004), Hydrogeomorphology: Overview of an emerging science, *Hydrol. Process.*, 18, 597–602.
- Soulsby, R. L. (1997), *Dynamics of Marine Sands*, pp. 249, Thomas Telford Publishing Services Ltd., London, U. K.
- Smith, R., and R. Hebbert (1983), Mathematical simulation of interdependent surface and subsurface hydrologic processes, *Water Resour. Res.*, 19, 987–1001.
- Smith, T. R., and F. P. Bretherton (1972), Stability and the conservation of mass in drainage basin evolution, *Water Resour. Res.*, 8, 1506–1529.
- Stephenson, G. R., and R. A. Freeze (1974), Mathematical simulation of subsurface flow contributions to snowmelt runoff, Reynolds Creek Watershed, Idaho, *Water Resour. Res.*, 10(2), 284–294, doi:10.1029/WR010i002p00284.
- Stock, J. D., and W. E. Dietrich (2003), Valley incision by debris flows: evidence of a topographic signature, *Water Resour. Res.*, 39(4), 1089, doi:10.1029/2001WR001057.
- Toth, J. (1963), A theoretical analysis of groundwater flow in small drainage basins, *J. Geophys. Res.*, 68(16), 4795–4812.
- Tucker, G. E., and R. L. Bras (1998), Hillslope processes, drainage density, and landscape morphology, *Water Resour. Res.*, 34, 2751–2764.
- VanderKwaak, J. E. (1999), Numerical simulation of flow and chemical transport in integrated surface-subsurface hydrologic systems, Ph.D. dissertation, 217 pp., Univ. of Waterloo, Waterloo, Ont., Canada.

MIRUS AND LOAGUE: HOW DOES RUNOFF BEGIN (AND END)?

- VanderKwaak, J. E., and K. Loague (2001), Hydrologic-response simulations for the R-5 catchment with a comprehensive physics-based model, *Water Resour. Res.*, 37, 999–1013.
- van Genuchten, M. Th., (1980), A closed-form equation for predicting the hydraulic conductivity of unsaturated soils, *Soil Sci. Soc. Am. J.*, 44, 892–898.
- Vereecken, H., R. Kasteel, J. Vanderborght, and T. Harter (2007), Upscaling hydraulic properties and soil water flow processes in heterogeneous soils: A review, *Vadose Zone J.*, 6, 1–28.
- Western, A. W., and R. B. Grayson (1998), The Tarrawarra data set: Soil moisture patterns, soil characteristics and hydrological flux measurements, *Water Resour. Res.*, 34, 2765–2768.
- Weiler, M., and J. McDonnell (2004), Virtual experiments: A new approach for improving process conceptualization in hillslope hydrology, *J. Hydrol.*, 285, 3–18.
- Yeh, T. J., M. Ye, and R. Khaleel (2005), Estimation of effective unsaturated hydraulic conductivity tensor using spatial moments of observed moisture plume, *Water Resour. Res.*, 41, W03014, doi:10.1029/2004WR003736.